ARTICLE

Daniel T. Maughan · Jeffrey D. Keith
Eric H. Christiansen · Tamalyn Pulsipher
Keiko Hattori · Noreen J. Evans

Contributions from mafic alkaline magmas to the Bingham porphyry Cu–Au–Mo deposit, Utah, USA

Abstract The Bingham porphyry Cu–Au–Mo deposit, Utah, may only be world-class because of substantial contributions of sulfur and metals from mafic alkaline magma to an otherwise unremarkable calc-alkaline system. Volcanic mafic alkaline rocks in the district are enriched in Cr, Ni, and Ba as well as Cu, Au, platinum group elements (PGE), and S. The bulk of the volcanic section that is co-magmatic with ore-related porphyries is dacitic to trachytic in composition, but has inherited the geochemical signature of high Cr, Ni, and Ba from magma mixing with the mafic alkaline rocks. The volcanic section that most closely correlates in time with ore-related porphyries is very heterogeneous containing clasts of scoriaceous latite, latitic, and minette, and flows of melanephelinite, shoshonite, and olivine latite in addition to volumetrically dominant dacite/trachyte. Bingham ore-related porphyries show ample evidence of prior mixing with mafic alkaline magmas. Intrusive porphyries that have not been previously well-studied have several chemical and mineralogical indications of magma mixing. These "mixed" lithologies include the hybrid quartz monzonite porphyry, biotite porphyry, and minette dikes. Even some of the more silicic latite and monzonite porphyries retain high Cr and Ba contents indicative of mixing and contain trace amounts of sapphire (< 1 mm). The heterogeneous block and ash flow deposits also contain sapphire and are permissively correlated with the intrusions based on chemical, mineralogical, and isotopic data. Magma mixing calculations suggest about 10% of the monzonitic/latitic orerelated magma may have been derived from mafic alkaline magma similar to the melanephelinite. If the original S content of the mafic magma was about 2,000–4,000 ppm, comparable with similar magmas, then the mafic magma may have been responsible for contributing more than half of the S and a significant portion of the Cu, Au, and PGE in the Bingham deposit.

Keywords Alkaline · Bingham · Mafic · Magma mixing · Porphyry Cu

Introduction

The Bingham Canyon Cu–Au–Mo porphyry is one of the largest porphyry copper deposits in the world (Ballantyne et al. 1997). The Bingham system is comprised of several small, mineralized stocks and dikes of Eocene age emplaced in Paleozoic quartzite and limestone, located about 30 km southwest of Salt Lake City, Utah (Fig. 1). A sequence of volcanic rocks of nearly identical age and similar petrographic and geochemical characteristics to Bingham porphyry intrusions lies 2–10 km south and east of the Bingham pit (Moore 1973; Lanier et al. 1978a; Moore and McKee 1983; Christiansen and Keith 1996; Deino and Keith 1997; Keith et al. 1997; Waite et al. 1997; Pulsipher 2000). Many workers have documented mineralization characteristics of the Bingham Cu–Au–Mo porphyry (Boutwell 1905; Lindgren 1924; Atkinson and Einaudi 1978; Lanier et al. 1978a, 1978b; Warnaars et al. 1978; Wilson 1978; Babcock et al. 1995; Phillips et al. 1997; Inan and Einaudi 2000; Redmond and Einaudi 2000). Others have documented petrologic, geochemical, isotope, and age relationships of various rock units of the Bingham district (Gilluly 1932; Moore 1973; Lanier et al. 1978a; Warnaars et al. 1978; Wilson 1978; Moore and McKee 1983; Babcock

D.T. Maughan · J.D. Keith (✉) · E.H. Christiansen · T. Pulsipher
Department of Geology,
Brigham Young University, Provo, Utah 84602, USA
E-mail: jeff_keith@byu.edu
Tel.: +1-801-3782189
Fax: +1-801-3788143

K. Hattori
Department of Earth Sciences,
University of Ottawa, Ottawa, Canada K1N 6N5

N.J. Evans
Ore Deposit Processes Group,
CSIRO Exploration and Mining,
North Ryde, NSW 1670, Australia

Fig. 1 *Shaded relief index map* of north-central Utah showing occurrences of Mid-Tertiary alkaline rocks (*black dots* and *boxes*). The *dashed line marks* the approximate trend of a poorly defined alignment of Middle Tertiary igneous rocks. This trend is parallel to but south of a proposed boundary between Archean and Proterozoic basements (Presnell 1997). Moon Canyon hosts lamproite intrusions and lava flows, and was used for a comparison of mica in Bingham district alkaline rocks
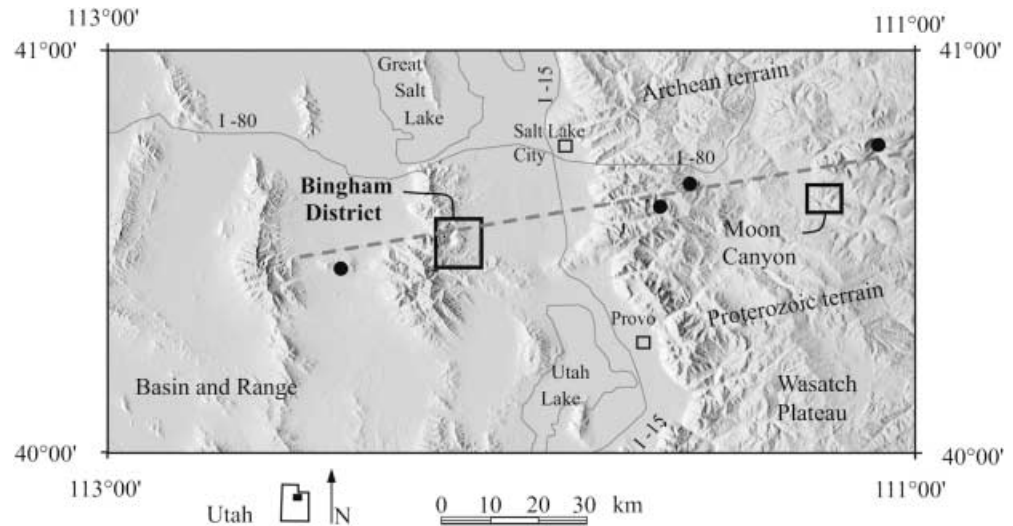
et al. 1995; Ballantyne et al. 1997; Deino and Keith 1997; Keith et al. 1997; Parry et al. 1997; Waite et al. 1997; Pulsipher 2000; Redmond and Einaudi 2000). Our work focuses on both newly discovered and previously documented (Gilluly 1932; Moore 1973; Moore and McKee 1983, Waite et al. 1997; Pulsipher 2000; Redmond and Einaudi 2000) mafic to intermediate alkaline rocks of the Bingham district. This study examines the role of the alkaline rocks that occur as both volcanic and intrusive phases in the mineralization of the Bingham district. The timing of their appearance in the volcanic and intrusive sequence indicates that they may have made substantial contributions of sulfur and metals to the ore-forming system. These alkaline mafic to intermediate rocks may be responsible, in part, for the unusual size and metal content of this world class Cu–Au–Mo system (Keith and Christiansen 1993; Waite et al. 1997; Keith et al. 1998).

Geologic setting

Several Eocene mineralized intrusions in northern Utah (including the Bingham Canyon Cu–Au–Mo porphyry system) occur along an E–W lineament called the Uinta–Cortez Axis (Roberts et al. 1965; Fig. 1). This lineament represents what some have considered an Archean–Proterozoic plate suture (Presnell 1997), although Pb and Nd model ages from Bingham district rocks suggest the presence of Proterozoic lithosphere (Stacy et al. 1968; Farmer and DePaolo 1983; Waite et al. 1997; Christiansen and Keith 2000). After suturing of the Archean–Proterozoic plates, a rifted continental margin formed, and Proterozoic and Paleozoic quartzites, shales, and limestones were deposited (Hintze 1988). Folding and thrusting of the Proterozoic and Paleozoic sedimentary rocks occurred during Jurassic Elko and Cretaceous Sevier orogenies (Presnell 1992, 1997; Constenius 1996). Presnell (1992, 1997) suggests that two episodes of extension occurred during the

Tertiary Period. Northeast-striking faults (possibly formed during the first episode of extension) host a significant portion of the vein-related late Eocene mineralization, implying that the faults were open at least during Bingham district mineralization, which occurred between 39.8 and 37.5 Ma (Warnaars et al. 1978; Deino and Keith 1997).

Host to the mineralization are late Eocene stocks and dikes, and Paleozoic sedimentary rocks. Some of the Eocene stocks and dikes apparently vented to the surface forming a composite volcano, part of which is preserved on the eastern flank of the Oquirrh Mountains (Moore et al. 1968; Moore 1973; Lanier et al. 1978a; Keith et al. 1997; Waite et al. 1997; Keith et al. 1998; Pulsipher 2000). This relationship is substantiated by (1) proximity of intrusive and extrusive rocks, (2) extrusive rocks dipping away from the Bingham intrusive center with steepest dips closest to the intrusive center to nearly horizontal at 10 km (Fig. 2), (3) similarities in mineralogy, texture, geochemistry, and isotopic compositions, and (4) radiometric ages.

Of particular interest is a section of block and ash flow deposits about 10 km south and east of the Bingham pit in Rose Canyon, which is closely correlated in time with Bingham mineralization and contains clasts of intermediate compositions that have experienced acid-sulfate alteration (clay, silica, jarosite, alunite, and barite) surrounded by unaltered ash and blocks (Pulsipher 2000). The rocks in this section also contain trace amounts of euhedral, accessory sapphire (< 1 mm), as do the quartz monzonite porphyry and other smaller intrusions in and around the Bingham deposit (Pulsipher 2000).

A younger magmatic event recorded by unmineralized dikes, stocks, and volcanic rocks followed with ages ranging from ~33 to ~30 Ma (Deino and Keith 1997; Waite et al. 1997). Subsequent Basin and Range extension (18 Ma–present) resulted in a $10.8 \pm 4.0°$ eastward tilt of the Bingham district since the late Eocene (Melker and Geissman 1997).

Fig. 2 Simplified geologic map of the eastern Oquirrh Mountains (after Laes et al. 1997) showing depositional strike and dip of volcanic units (corrected for post-volcanic regional tilt), in relation to Bingham intrusive units. A line encompassing the Bingham deposit represents Cu contents > 0.35 wt% at the 5,000-foot level of the mine
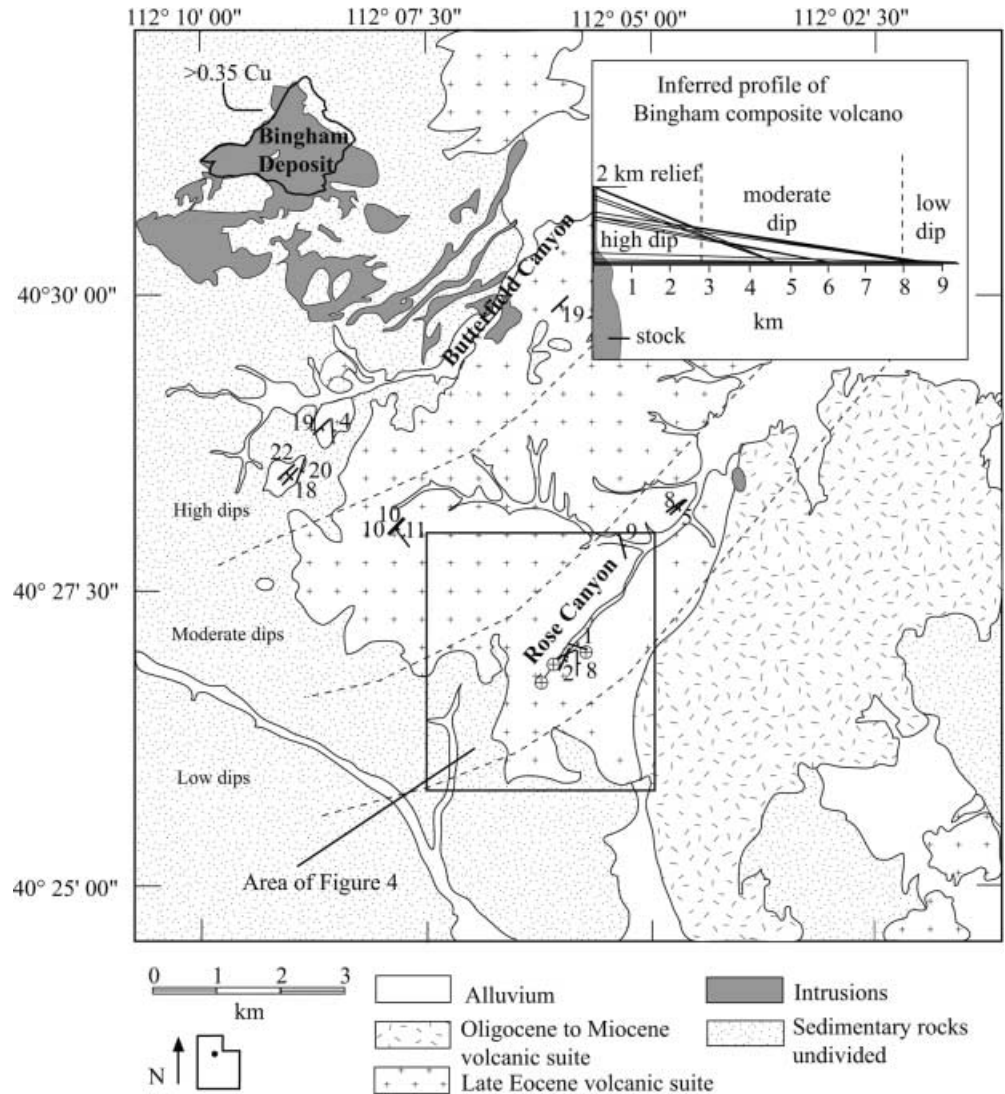
Sampling and analytical methods

A total of 103 samples were collected for this study of the Bingham district. Of these, 17 samples came from relatively mafic intrusions in the Bingham deposit and 86 came from pyroclasts found in block and ash flows, lava flows, and mafic dikes in and near Rose Canyon. The data from these samples were combined with data from Pulsipher (2000; 60 samples); Waite et al. (1997; 91 samples) and Barr (1993; 4 samples) for a total of 258 samples.

The 103 samples collected for this study focus on the mafic to alkaline rocks of the Bingham district. By alkaline, we mean containing sufficient total alkali content to place samples in or above the basanite, trachybasalt, shoshonite, latite, and trachyte fields on the International Union of Geological Scientists (IUGS) classification diagram for volcanic rocks (Fig. 3; Le Maitre 1989). Phenocrystic plagioclase is absent or sparse in most of the 103 alkaline samples. Only the melanephelinite is significantly silica undersaturated and contains no CIPW normative albite. Some shoshonite lavas are silica undersaturated and contain modest amounts of CIPW normative nepheline whereas other shoshonites do not.

Most samples collected outside of the Bingham open pit were neither significantly weathered nor hydrothermally altered. Samples from within the Bingham pit show minor to significant hydrothermal alteration, but no significant weathering. Standard or polished thin sections were made from most of the samples for petrographic descriptions. Detailed petrographic descriptions and other data not tabulated in this paper can be found in Maughan (2001).

Samples were powdered in a tungsten carbide shatter box, and dried overnight in an oven at 105 °C. Glass disks were prepared by fusing rock powder with a 50/50 mixture of Spectroflux 105-lithium tetraborate and metaborate flux, and analyzed to determine major element compositions of the samples. Rock powders were pressed into pellets backed by Whatman fibrous cellulose powder, and analyzed to determine trace element concentrations. Major and trace element abundances were determined at BYU on a Siemens SRS-303 X-ray fluorescence spectrometer (XRF). Multiple analyses of international standards can be found in Maughan (2001) and measured precision and accuracy of the analyses.

Rare earth elements (REE), Mo, Ag, Sb, Hg, and Bi element abundances were determined by Chemex Labs using inductively coupled plasma mass spectrometry (ICP-MS). Platinum group element and gold analyses were performed at CSIRO Exploration and Mining by isotope dilution and external calibration ICP-MS (method in Evans et al. 1993). Gold abundances were also determined at Chemex Labs by fire assay and atomic absorption methods.

Mineral compositions in a representative suite of samples were determined at BYU with a Cameca SX50 electron microprobe (upgraded to SX100 standards) with a 20-nA beam and 15.0-kV acceleration voltage.

Fig. 3 IUGS chemical classification of volcanic rocks (Le Maitre 1989) for Bingham intrusive and extrusive rocks. We regard alkaline rocks to plot above the line separating andesite from latite and its projection. Intrusive rocks from the Bingham pit commonly exhibit potassic alteration and silicification
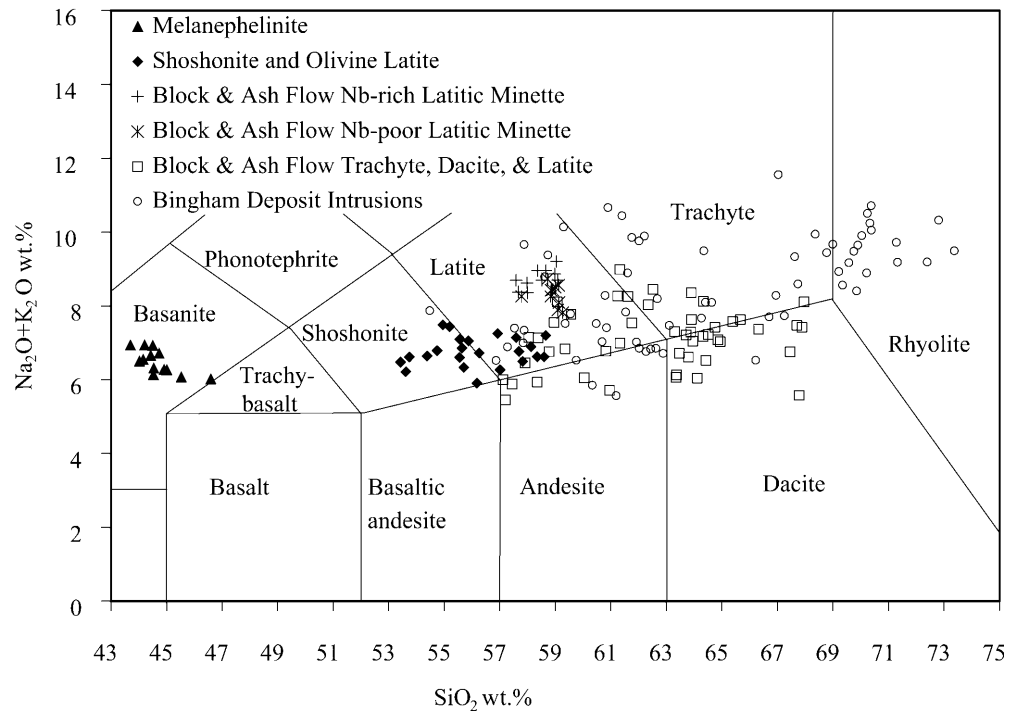
For Nd and Sr isotopic analysis completed at the University of Ottawa, samples were digested using a mixture of HF–HNO$_3$–HClO$_4$ in Savillex screw-top Teflon vials at 200 °C for >24 h. Samples were then dried at 150 °C and raised to 200 °C to remove HClO$_4$ and reacted with 6 N HCl, followed by evaporation to dryness. This was repeated twice and the sample was dissolved in 2.5 N HCl for cation separation using Bio Rad AG 50 W-X8 (200–400 mesh). Neodymium and Sm were separated using a Teflon powder resin coated with di-ethylhexyl orthophosphoric acid. Total chemical blanks are <0.1 ng for Nd and <0.05 ng for Sr, which are negligible in comparison to the amounts of Sr and Nd present in the samples. HCl was double distilled in Teflon distillation vessels at sub-boiling temperatures. Double distilled HF and HClO$_4$ were purchased from Seastar Chemicals. Isotopic measurements were made on a multi-collector thermal ionization mass spectrometer (Finnigan MAT 261), and the ratios for Sr and Nd isotopes were normalized to $^{86}Sr/^{88}Sr$ of 0.1940 and $^{146}Nd/^{144}Nd$ of 0.7219. Isotopic analysis of NBS987 gave $^{87}Sr/^{86}Sr$ of 0.710257 ± 14 ($n = 14$) and those of La Jolla $^{143}Nd/^{144}Nd$ of 0.511866 ± 16 ($n = 8$). Concentrations of Sr, Rb, Nd, and Sm were determined by isotopic dilution technique using mixed spikes of ^{84}Sr–^{87}Rb and ^{148}Nd–^{149}Sm added to the samples before digestion.

Correlation of intrusive and extrusive units in the Bingham district

In 1992, fieldwork and sample collection commenced in the Bingham district with the intention of examining the possibility that some of the Bingham intrusions may have erupted and created the volcanic deposits of the district. Prior work by Moore (1973) and others suggested that possibility. In addition, Moore (1973) suggested that of all the Bingham intrusions, the amphibole-bearing latite dikes most closely match the composition of some volcanic rocks in the 1-km-thick volcanic section. Our initial studies verified this broad observation (Keith et al. 1997; Waite et al. 1997). Additionally, we

found that both the Bingham district intrusions (using the least altered samples) and volcanic rocks of the same age were abnormally rich in Cr and Ba compared with other Tertiary volcanic centers in central Utah and the Great Basin.

Most of the Bingham intrusions are steep-walled intrusions that may have vented just as readily as the coeval latite dikes noted by Moore (1973). Thus a more careful examination was conducted of that portion of the volcanic section that most closely correlated in time with the ore-related intrusions. Mineralized minette dikes (37.74 ± 0.11 Ma) within the ore body have the same age as the youngest ore-related intrusion – the quartz latite porphyry (37.72 ± 0.09 Ma). These ages are indistinguishable from that of the melanephelinite flow in Rose Canyon (37.84 ± 0.14 Ma; Deino and Keith 1997) about 10 km south of the Bingham deposit.

Pulsipher (2000) found that trace amounts of sapphire crystals (<1 mm in diameter) are present in the quartz monzonite porphyry, nearby latite porphyry dikes from Butterfield Canyon (Fig. 2), latitic minette clasts from block and ash flow deposits, and the ash and pumice portion of the block and ash flows. Taken together, these unusual characteristics strongly argue for a co-magmatic origin for the volcanic and intrusive rocks. Precise correlations based on radiometric age, mineralogy, or chemical compositions are difficult because of the overprinted effects of hydrothermal alteration. The estimated pre-alteration mineralogy and chemical composition of the quartz monzonite porphyry (the largest and earliest ore-related intrusion) is permissively correlative with these dacitic quartz-bearing pumice lapilli. This does not mean that there is a one-to-one correlation between emplacement of the block and ash flow unit and

intrusion of the quartz monzonite porphyry – only that they are likely to be co-magmatic. This is because small volume eruptions may have occurred for which no intrusive vestige remains behind after subsequent eruptions and intrusions used the same vent.

It is important to note that eruptions do not consist of uniform dacitic or trachytic compositions. Instead, the quartz- and sapphire-bearing block and ash flows are heterogeneous and also contain clasts of alkaline rocks e.g., olivine-bearing latite and shoshonite scoria (Fig. 4). Lava flows of shoshonite and melanephelinite are intercalated with, and post-date, this eruptive sequence. These more mafic components of the Bingham system, and their potential contributions to ore formation, are the focus of this paper.

Bingham stock emplacement sequence

Redmond and Einaudi (2000) describe five separate mineralizing intrusions in the Bingham deposit, all hosted by an older equigranular monzonite, limestone, skarn, or quartzite. From oldest to youngest they are quartz monzonite porphyry (80% of the volume of ore-forming intrusions), latite porphyry (12%), biotite porphyry (1%), quartz latite porphyry breccia (2%), and quartz latite porphyry (about 5% of the volume of ore-forming intrusions). These units represent those encountered during Redmond and Einaudi's (2000) mapping of portions of two benches in the Bingham pit. In addition, two other small ore-related intrusive units are present in the Bingham deposit – namely, the hybrid quartz monzonite porphyry and minette dikes. Hybrid quartz monzonite porphyry is located between quartz monzonite porphyry and equigranular monzonite; this hybrid was originally proposed to represent assimilation of equigranular monzonite by the quartz monzonite porphyry magma (Lanier 1978a; although other hypotheses of origin are discussed in a later section). At least two narrow minette dikes are present in the Bingham deposit, one of the dikes was dated by Deino and Keith (1997) at 37.74 ± 0.11 Ma. About 1–2 km south and east of the Bingham deposit are coeval amphibole- and sapphire-bearing, sulfide-rich latite dikes, and pre-mineralization equigranular monzonite of the Last Chance stock.

Fig. 4 Geologic map of Rose Canyon, Utah, approximately 10 km south of the Bingham Cu–Mo–Au porphyry deposit. Volcanic rocks in Rose Canyon are indistinguishable in age from Bingham intrusions (Warnaars et al. 1978; Deino and Keith 1997). Many clasts in the volcanic units exposed in Rose Canyon have similar compositions to rock types found in the Bingham deposit; others are altered to alunite, whereas still others may represent a relatively primitive parent magma for the Bingham intrusions
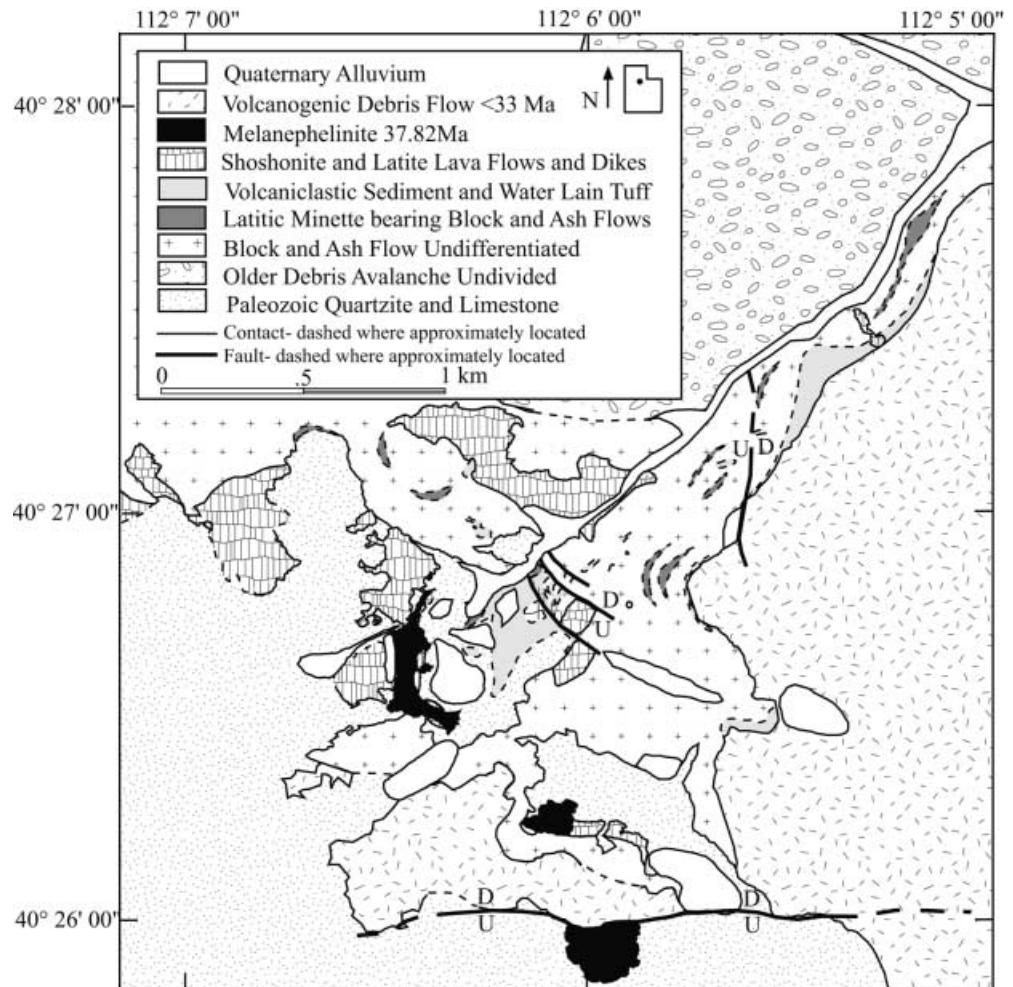
Rose Canyon stratigraphy

Pulsipher (2000) used several lines of reasoning to show that current-day Rose Canyon was likely near the toe of a composite volcano that was centered over the Bingham intrusions 38 million years ago (Fig. 2) at a time when small-volume block and ash flow deposits and mafic lava flows were still being erupted. The block and ash flow deposits often swell and pinch rapidly and are laterally traceable only to a limited extent (Fig. 4). At least nine individual block and ash deposits can be distinguished. The entire sequence of lava flows and block and ash flows varies between 100 and 350 m in the central and northwestern portions of Rose Canyon. The volcanic sequence in Rose Canyon is largely bracketed by two ages: 38.68 ± 0.13 Ma from sanidine in the basal block and ash flow (A. Deino, personal communication 2001) and 37.84 ± 0.14 Ma for the melanephelinite flow (Deino and Keith 1997). These ages may also bracket the time of emplacement for most, or all, of the five ore-related Bingham intrusions.

Clast composition, texture, mineralogy, abundance of ash, and sorting help distinguish individual block and ash flow units. Clast compositions in the block and ash flow unit, in order of decreasing abundance, consist of (1) breadcrust-textured dacite and trachyte, (2) scoriaceous to pumiceous latite, (3) latitic minette, (4) quartzite, and (5) hydrothermally altered dacite. Field relations clearly show that some clasts (<1%) were altered prior to their emplacement in the Rose Canyon area, possibly as a result of fumarolic or hot spring activity near the eruptive source. Alteration products include clay, porous silica, alunite, jarosite, and barite.

With such heterogeneous deposits, it is difficult to ascertain which clasts represent juvenile erupted material and which were simply entrained during eruption and transport. Breadcrust-textured dacite and trachyte clasts are usually the most abundant clasts in individual deposits and are likely juvenile material. The blocks were probably derived from a still-hot(?) dacitic to trachytic dome complex that collapsed as result of dacitic pumice and ash eruption. This is indicated by the fact that most block and ash flow deposits display normal sorting. Consequently, pumice and ash are likely juvenile. Portions of some block and ash flows, or individual block and ash flows, are dominated by mafic clasts and scoria (as discussed below). The southwestern portion of Rose Canyon is dominated by rocks that accumulated in a slightly younger paleovalley incised into the block and ash flow deposits and Paleozoic rocks. The paleovalley is filled with volcaniclastic sediments and mafic lava flows (Fig. 4).

Unit descriptions

Melanephelinite

The most mafic rock type found in the Bingham district has been variously named by different workers (for instance, Gilluly 1932). Essentially the same lithology has been classified as mafic minette, olivine nephelinite, nepheline basalt, and melanephelinite (Fig. 3). According to the IUGS chemical classification scheme for nephelinitic rocks (Le Bas 1989), they are olivine melanephelinites with no normative albite and less than 20% normative nepheline. This term is used to emphasize their low Al_2O_3 content ($\sim$10.30 wt%) and distinctively sodic character, which contrasts with the generally potassic rocks of the remainder of the volcanic field.

The melanephelinite has a whole-rock $^{40}Ar/^{39}Ar$ plateau age of 37.82 ± 0.14 Ma (Deino and Keith 1997). Melanephelinite lava flows with subordinate shallow dikes and breccia are present in a single exhumed paleovalley in at least three different locations in the Rose Canyon vicinity (Fig. 4). The southern most outcrop is probably all massive lava flow in unconformable contact with Paleozoic quartzite. The two northern outcrops contain both massive and brecciated melanephelinite, which occurs as near surface dikes, plugs, and lava flows.

Olivine (Fo_{91}–Fo_{87}; Fig. 5; Table 1) is the most abundant phenocryst, making up 18–25 vol% of the rock. Minor phlogopite is often present as phenocrysts or in the matrix. Phlogopite phenocrysts (up to 2 cm) are oxidized and partially resorbed, and are rimmed with small grains of Fe–Ti oxide and nepheline and contain mostly water in the hydroxyl site (Table 2). Phlogopite site occupancy calculations commonly show vacancies in the tetrahedral site (Fig. 6). Analyses of the freshest phlogopite phenocrysts yield temperatures of $1,140 \pm 43$ °C according to the Ti-geothermometer of Righter and Carmichael (1996). Ba concentrations range widely, implying equilibration over a wide range of
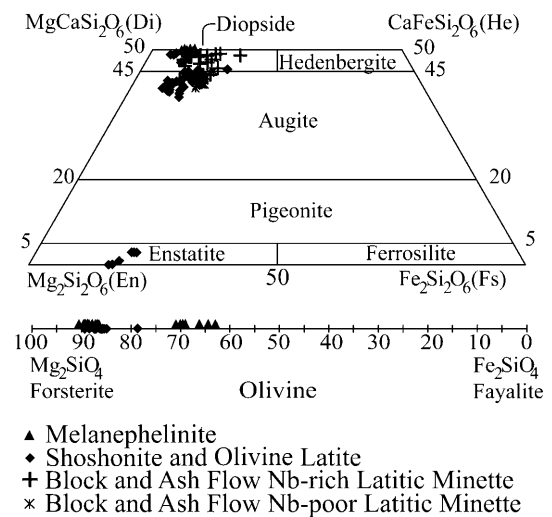
Fig. 5 Pyroxene and olivine compositions of volcanic rocks of Rose Canyon. Melanephelinite and Nb-rich latitic minette contains diopside, Nb-poor latitic minette, and shoshonite, and olivine latite contains diopsidic augite to diopside. Olivine latite contains minor amounts of opx as exsolution lamella in clinopyroxene, and as rare crystals in inclusions. Olivine compositions lie between Fo_{91}–Fo_{84}. Some of the melanephelinite olivine crystals have 25–50-μm-wide Fo_{72}–Fo_{63} rims. Latitic minette contains no olivine

Table 1 Representative olivine compositions from melanephelinite and shoshonite of Rose Canyon

wt%	Melanephelinite			Shoshonite	
	Tick-103			Lowe-21A Core	Tick-116 Core
	Core	Near edge of rim	Edge of rim		
SiO_2	40.829	40.490	36.512	40.247	39.819
TiO_2	0.007	0.013	0.007	0.019	0.000
Al_2O_3	0.010	0.022	0.021	0.035	0.003
FeO	8.984	10.672	30.400	12.047	13.118
MnO	0.129	0.133	1.164	0.220	0.178
MgO	49.323	47.376	31.539	46.997	45.740
CaO	0.113	0.142	0.279	0.185	0.239
NiO	0.406	0.341	0.095	0.183	0.215
Total	99.801	99.189	100.017	99.933	99.312
Formula unit based on four oxygens					
Si	1.000	1.005	0.994	0.998	0.999
Ti	0.000	0.001	0.001	0.001	0.000
Al	0.000	0.000	0.000	0.000	0.000
Fe	0.184	0.222	0.692	0.250	0.275
Mn	0.003	0.003	0.027	0.005	0.004
Mg	1.801	1.753	1.280	1.738	1.711
Ca	0.003	0.004	0.008	0.005	0.006
Ni	0.008	0.007	0.002	0.004	0.004
Total	2.999	2.995	3.004	3.001	2.999
End members					
Mo	0.149	0.191	0.409	0.248	0.323
Fo	90.742	88.825	64.295	87.442	86.256
Fa	9.272	11.224	34.765	12.574	13.878
Li	0.403	0.345	0.104	0.184	0.219
Te	0.135	0.141	1.349	0.232	0.190
(Fe + Mn) (Fe + Mn + M)	9.393	11.344	35.967	12.774	14.022

pressures (Righter and Carmichael 1996) and are not considered meaningful. Phlogopite in the matrix (although not present in all samples) poikilitically encloses all other matrix phases, contains mostly F in the hydroxyl site (5.98 wt% F; Table 2), and is not dusted with Fe–Ti oxides. Calculated crystallization temperatures (about 1,075 °C) and pressures (many give negative results– probably because of the difficulty in estimating the Ba content of the coexisting liquid) are lower than for phenocrystic phlogopite. Clinopyroxene, Fe–Ti oxides, apatite, and minor amounts of nepheline comprise the remainder of the matrix of the melanephelinite (Fig. 5, Table 3).

Inclusions in olivine consist of phlogopite, magnesiochromite, barite, and apatite and may appear together in the same inclusion or separately. These inclusion relationships suggest that both barite and phlogopite may have been more abundant in the magma prior to eruption and degassing. These phases may have crystallized in a barium- and sulfate-rich boundary layer surrounding growing olivine. The oxygen fugacity of these flows was estimated by Tomlinson et al. (2000) to be about 2 log units above the NNO buffer (ΔNNO = 2) based on measured ferric/ferrous iron ratios of five samples. The melanephelinite is the only igneous rock type of the Bingham district that lacks blebs of magmatic sulfide (but may contain magmatic sulfate).

The melanephelinite flows and intrusions of Rose Canyon are geochemically and mineralogically distinct from most melanephelinites in several important ways. For example, phlogopite is a common phenocryst and groundmass phase. Compared with the average melanephelinite compositions presented by Le Bas (1989), these rocks have distinctly lower TiO_2 (1% versus 3–4%), lower P_2O_5, and higher Mg/Fe ratios. Most melanephelinites also have trace element patterns that peak at Nb and lack Ti depletions. In contrast, the Bingham melanephelinites have marked negative Nb and Ti anomalies (Fig. 7), even though they are enriched in Nb compared with most Bingham district rocks (Fig. 8, Table 4).

The melanephelinites of the Bingham district are its most geochemically distinctive rocks. Not only are they the most primitive in terms of the mantle-compatible elements Cr, Ni, Sc, Fe_2O_3, and MgO, but they also have high concentrations of mantle-incompatible elements, especially large ion lithophile elements (LILE) such as Ba, Rb, K, and Sr. Fluorine concentrations are also high, ranging from 3,000 to 7,000 ppm (Table 4). The melanephelinites also have the highest concentrations of Nb of any igneous rocks thus far analyzed from the district. Rare earth element patterns show the enrichment of light REE, but the slope of the pattern is relatively shallow ($Ce/Yb_N \cong 10$). In addition, the trace element pattern

Table 2 Representative mica compositions from melanephelinite, latitic minette of Rose Canyon, minette dike of the Bingham deposit, and lamproite from 100 km east of the Bingham deposit in Moon Canyon

	Melanephelinite		Latitic Minette		Bingham	Moon
	Tick-43		Nb-rich Tick-79 core	Nb-poor Tick-52A rim	Minette Bing-40 interior	Canyon Lamproite core
	Pheno core	Poikilitic				
SiO$_2$	39.486	40.473	38.886	37.453	38.121	40.985
TiO$_2$	1.341	2.336	2.991	3.403	2.603	2.397
Al$_2$O$_3$	14.320	11.021	14.163	14.021	14.778	12.203
Cr$_2$O$_3$	0.877	0.000	0.350	0.052	0.047	0.824
FeO	4.853	5.064	9.755	11.328	14.033	3.025
MnO	0.000	0.092	0.046	0.032	0.080	0.032
MgO	23.042	23.332	19.008	18.140	16.513	25.378
CaO	0.000	0.033	0.002	0.000	0.000	0.000
Na$_2$O	0.260	0.351	0.350	0.744	0.179	0.213
K$_2$O	10.533	10.082	9.985	9.263	9.264	10.389
BaO	0.272	2.221	0.475	1.042	0.304	0.038
F	0.880	5.981	1.244	1.800	0.590	1.826
Cl	0.043	0.000	0.019	0.137	0.239	0.005
H$_2$O[a]	3.686	1.202	3.449	3.096	3.680	3.321
Total	99.211	99.670	100.195	99.722	100.127	99.866
Grams per formula unit						
Normalized to 7 octahedral + tetrahedral cations						
Si	2.876	3.004	2.881	2.816	2.841	2.931
Ti	0.074	0.130	0.166	0.192	0.146	0.129
Al	1.229	0.964	1.237	1.243	1.298	1.029
Cr	0.025	0.000	0.010	0.001	0.001	0.023
Fe	0.295	0.314	0.605	0.712	0.875	0.181
Mn	0.000	0.006	0.003	0.002	0.005	0.002
Mg	2.501	2.581	2.098	2.033	1.834	2.705
Ca	0.000	0.003	0.000	0.000	0.000	0.000
Na	0.037	0.050	0.050	0.108	0.026	0.030
K	0.978	0.955	0.944	0.889	0.881	0.948
Ba	0.008	0.065	0.014	0.031	0.009	0.001
F	0.203	1.404	0.292	0.428	0.139	0.413
Cl	0.005	0.000	0.002	0.018	0.030	0.001
OH[a]	1.792	0.596	1.706	1.554	1.831	1.586
End member						
phlog	0.841	0.852	0.702	0.678	0.612	0.897
sid	0.060	0.000	0.114	0.135	0.180	0.009
annite	0.099	0.158	0.184	0.187	0.208	0.094

[a]Indicates water and OH concentrations calculated by using Munoz (1981)

shows the characteristic depletions of high-field strength elements (HFSE) found in many orogenic magma series. Although not potassic (Na$_2$O wt% exceeds K$_2$O wt% for all samples), the compositions of the melanephelinites generally fall in the arc fields on the discriminant diagrams of Müller and Groves (2000). The only exception is caused by their low Al content. Perhaps of most significance here, however, are the relatively high concentrations of Cu found in the melanephelinite, ranging from 90 to 130 ppm. This is higher than any of over 300 middle Tertiary mafic to intermediate rocks from the Great Basin analyzed by Barr (1993).

As expected from their mafic character, platinum group elements (PGEs) are also enriched in the melanephelinites (Fig. 9 and Table 5). The lowest melting point PGE (Pd) and Au are strongly enriched compared with depleted mantle. Concentrations and patterns are similar to shoshonitic systems like those of Fiji and Lihir, Papua New Guinea with the exception that concentrations of Ru, Ir, and Rh are higher in the Bingham melanephelinites by factors of 2–10. Enrichment of these refractory PGEs may be caused by the relatively high temperature of the alkalic magma and its rapid rise to the surface without fractionation of chromite or other phases that may contain refractory PGEs.

Initial ^{87}Sr/^{86}Sr isotope ratios and ϵNd (38 Ma) for the melanephelinite are the most primitive in the Bingham volcanic field (i.e., 0.7072 and 0.7069 and –7 and –8, respectively, Table 6). In spite of their primitive character, they fall off the mantle array (Fig. 10) and indicate crustal contamination or an anomalous mantle source.

Shoshonite/olivine latite

One sequence of lava flows (rarely found as block-and-ash-flow clasts) that exhibits a coherent set of mineralogical and chemical characteristics is the shoshonite/
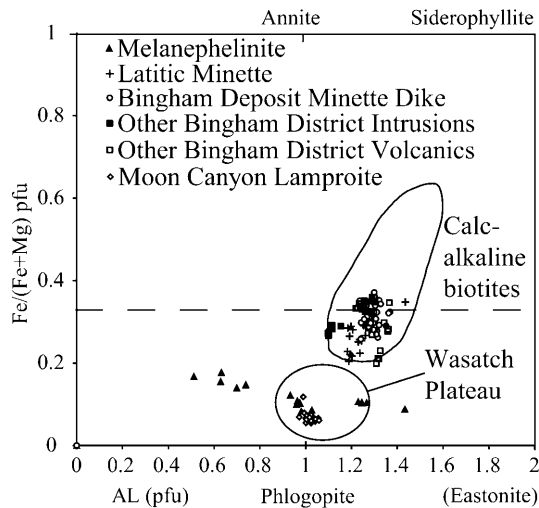
Fig. 6 Mica compositions in relatively fresh intrusive and extrusive rocks from the Bingham district. Most mica compositions are similar to biotite from other calc-alkaline igneous rocks (Christiansen et al. 1986). Micas from the melanephelinite are distinctly phlogopitic and are often depleted in Al (Maughan et al. 1999), as found in other alkaline rocks (Rock 1991) including the 38.4-Ma Moon Canyon lamproite (Best et al. 1968; Fig. 1) and late Oligocene minettes from the Wasatch Plateau (Tingey et al. 1991; Fig. 1)

olivine latite group (Fig. 3). Melanephelinite outcrops are spatially and temporally proximal to small shoshonite and olivine latite dikes, breccia, and lava flows (Fig. 4). Some shoshonite and olivine latite lavas lie directly above melanephelinite. The predominant exposures of the shoshonite/olivine latite are as oxidized, red "aa"-type lava flows. Phenocrysts are typically smaller than 2 mm, and are not as abundant in the dikes as they are in the lava flows. Absolute and relative age relationships show the shoshonite/olivine latite lava flows were erupted several times between about 39 to 37.8 million years ago (Fig. 4).

This group straddles the boundary between shoshonite and latite (Fig. 3). In contrast to the melanephelinite, these are potassic rocks with K_2O wt% exceeding Na_2O wt%. Two distinctive groups (shoshonite and olivine latite) are apparent upon thin-section inspection and by comparing Ni abundances. The shoshonite samples typically have lower silica and higher alkali contents than olivine latite. Shoshonite Ni abundances are relatively low with seven samples averaging 78 ppm. On most diagrams, the shoshonites trend toward the latitic minettes described below (Figs. 3 and 11). On the other hand, the olivine latites are less alkaline, have higher silica, but less Nb and more Ni (greater than 150 ppm Ni) than the shoshonites (Figs. 3, 8, and 11, Table 4). For both types, the MgO/(MgO + FeO) ratios calculated using ferric iron concentrations measured by Tomlinson et al. (2000) are also high, exceeding 0.7 in all cases. Nb and Ti are not as enriched in the shoshonite and olivine latite as in the melanephelinite, and they are less enriched in LREE than the melanephelinites (Fig. 7).

All members of this group have olivine phenocrysts in spite of their intermediate silica contents (SiO_2 52–59 wt%; Fig. 3). Olivine phenocrysts are small, < 2 mm, have compositions ranging from Fo_{88}–Fo_{84} (Fig. 5), and constitute up to 25 vol% of the rock. Olivine in the shoshonites is slightly more Mg-rich than in the olivine latites. Olivine crystals contain small inclusions of magnesiochromite. Samples from the shoshonitic end of the compositional spectrum typically contain less olivine, but more clinopyroxene than the latite samples. The olivine latite has up to 25% small, sharply euhedral and flow aligned olivine (Fo_{86}–Fo_{84}) phenocrysts. Augitic clinopyroxene phenocrysts (Fig. 5, Table 3) account for 2–10 vol% of the shoshonite and olivine latite. Very small crystals of feldspar are present in the matrix of some samples whereas others have none. Fe–Ti oxides and a few magmatic sulfide blebs are present in the matrix and as inclusions in clinopyroxene. Only one shoshonite was analyzed for its ferrous–ferric iron content and it yielded ΔNNO of + 1.5; latite samples scatter from 2 to as much as 6 log units above the NNO oxygen buffer (Tomlinson et al. 2000).

The analyzed shoshonite has initial $^{87}Sr/^{86}Sr$ values of ~0.7088 and ϵNd (38 Ma) of –16.1 (Table 6), which is considerably more enriched than the melanephelinites. Two samples of olivine latite have even higher initial $^{87}Sr/^{86}Sr$ and lower ϵNd (38 Ma). These isotopic values are consistent with considerable crustal contamination. The Nd model ages lie between 1.7 and 1.9 Ga.

Black or white quartzite xenoliths as large as 4 cm in diameter are found in the shoshonite/olivine latite. Igneous inclusions, of cognate or xenolithic origin, are as large as 8 cm and consist largely of clinopyroxene, with less and varying amounts of orthopyroxene, phlogopite, olivine, and magnesiochromite. The inclusions have SiO_2 that varies between 50–54 wt%, MgO values as high as 18 wt%, 3,200 ppm Cr and 900 ppm Ni. The inclusions rather high concentrations of Al, Ti, Ca, and Na (of about 6.5, 0.7, 8.5, and 1.2 wt% respectively) and relatively low Mg and Ni (peridotite xenoliths have around 40 wt% Mg and 2,400 ppm Ni) argue that they were not derived from the mantle. They are more likely cumulates crystallized from contaminated magmas as argued below.

Scoriaceous latite pyroclasts

Scoriaceous latite clasts are present in the ash and pumice-rich upper part of the block and ash flow deposits. They appear to be primary magmatic products co-erupted with the dacitic ash and pumice. They have more evolved compositions (more silica and typically lower contents of compatible elements) than the olivine latite, but they have lower total alkalies than latitic minette (Fig. 3). Some are andesites on the TAS diagram (Fig. 3). Silica abundances range between 57–59 wt%, Cr abundances are up to 500 ppm, but more typically between 40 and 150 ppm (Fig. 11). Nickel abundances

Table 3 Representative pyroxene compositions from melanephelinite, shoshonite, and latitic minette of Rose Canyon

wt%	Melanephelinite Tick-103 core	Shoshonite Tick-116 core	Latitic Minette	
			Nb-rich Tick-79 rim	Nb-poor Tick-52A core
SiO_2	52.276	54.234	53.810	51.861
TiO_2	0.467	0.177	0.309	0.455
Al_2O_3	1.315	1.710	0.922	2.178
Cr_2O_3	0.452	0.367	0.084	0.005
FeO	3.945	4.712	4.421	8.600
MnO	0.120	0.140	0.097	0.378
MgO	15.746	17.732	16.458	15.260
CaO	24.379	20.428	23.032	20.440
Na_2O	0.369	0.397	0.281	0.383
Total	99.069	99.897	99.414	99.560
Formula unit based on six oxygens				
Si	1.943	1.973	1.980	1.935
Ti	0.013	0.005	0.009	0.013
Al	0.057	0.073	0.040	0.096
Cr	0.040	0.011	0.002	0.000
Fe	0.123	0.143	0.136	0.269
Mn	0.004	0.004	0.003	0.012
Mg	0.873	0.962	0.903	0.849
Ca	0.971	0.796	0.908	0.817
Na	0.026	0.028	0.020	0.028
Total	4.049	3.995	4.001	4.018
End member				
Wo	0.494	0.419	0.466	0.422
En	0.444	0.506	0.464	0.439
Fs	0.062	0.075	0.07	0.139

occur between 20 and 70 ppm and total alkali contents range between 6–8 wt% (Fig. 3).

Phenocrystic biotite makes up around 5% or less of each sample whereas clinopyroxene is usually slightly more abundant. Phenocrystic plagioclase is typically sparse or absent. Some scoriaceous latite clasts have matrices dominated by plagioclase, whereas others have very little matrix plagioclase and are glassy. Vesicles can be as large as 2 cm and often define a strong flow lineation. A latite pyroclast (Tick-55A) in the block and ash flow deposit has ϵNd (38 Ma) values of –17.9 and initial $^{87}Sr/^{86}Sr$ values of 0.7102 (Table 6).

Latitic minette

Some latite clasts in block and ash flow contain up to 20% mica (ranging from Fe-rich phlogopite to biotite) phenocrysts, with lesser but variable amounts of clinopyroxene, and no phenocrystic feldspar. Because of the abundance of mica and lack of phenocrystic feldspar, these clasts can be classified as minette (using lamprophyre nomenclature), or in this case, latitic minette.

Latitic minette occurs as violet-brown to gray or black, weakly vesicular, mica- and clinopyroxene-bearing (diopside to augite), phenocryst-rich clasts in the block and ash flow unit (Fig. 4). No dikes or lava flows of latitic minette are known in the area, but attitudes of bedding and unit contacts suggest a source to the north towards the Bingham intrusions (Fig. 2; Pulsipher 2000). Typical block and ash flow contains only a few percent latitic minette clasts with the dominant portion of block and ash flow clasts consisting of dacite, latite, and trachyte in an ash and pumice-bearing matrix (Pulsipher 2000). Individual block and ash flow deposits may consist of 90–100% latitic minette clasts. These few unusual deposits, rich in latitic minette, swell and pinch but are laterally traceable in Rose Canyon for distances up to 1 km (Fig. 4).

A total alkali-silica (TAS) diagram distinguishes the latitic minette from other rock groups of the Bingham district with the total alkali content of the latitic minette ranging between 8.1 and 9.2 wt% (Fig. 3) and 57.5 to 59 wt% SiO_2. Like the shoshonites, these are distinctly potassic rocks and lack normative nepheline. Two groups of latitic minette are apparent on a Nb vs. Zr (Fig. 8) variation diagram. One (Nb-rich latitic minette) has distinctly higher Nb, Zr, and other trace element abundances (Fig. 7, Table 4). The other (Nb-poor latitic minette) is typically about 0.5 wt% richer in silica than is Nb-rich latitic minette. Cr abundances of Nb-poor latitic minette range from 70 to 100 ppm whereas Cr abundances of Nb-rich minette range from 130 to170 ppm (Fig. 11, Table 4). Field relations show that the Nb-rich latitic minette clasts probably occur at a slightly higher (younger) stratigraphic interval in the block and ash flow than the Nb-poor latitic minette. Despite the relative enrichment of high field strength
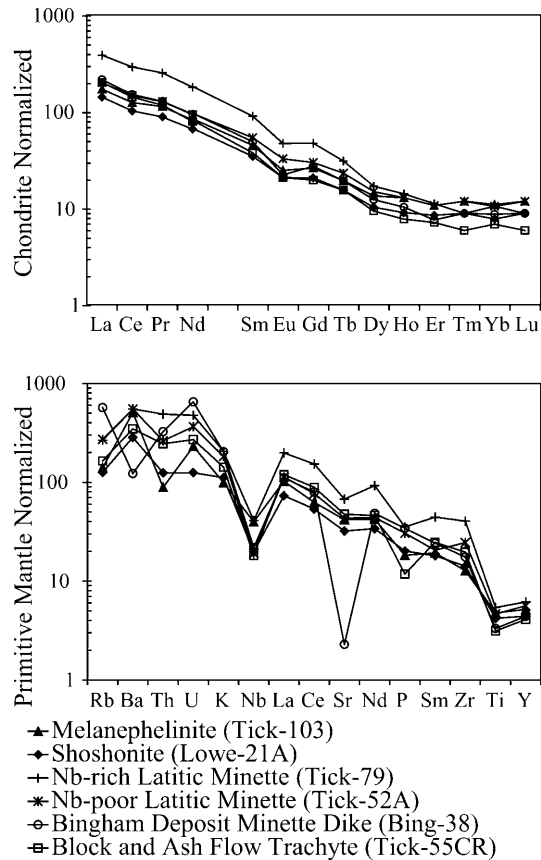
Fig. 7 Chondrite-normalized rare earth element diagram (Nakamura 1974) and primitive mantle-normalized trace element diagram (McDonough and Sun 1995) for representative samples from the Bingham district. Alteration removed significant amounts of Sr and Ba, and added K and Rb to samples collected from the Bingham pit

▲ Melanephelinite
◆ Shoshonite & Olivine Latite
+ Block & Ash Flow Nb-rich Latitic Minette
✗ Block & Ash Flow Nb-poor Latitic Minette
□ Block & Ash Flow Trachyte, Dacite, & Latite
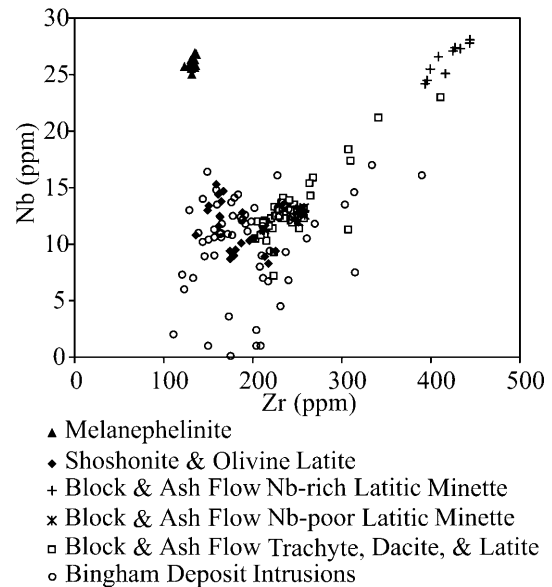○ Bingham Deposit Intrusions

Fig. 8 Variation of Nb versus Zr for Bingham intrusive and extrusive rocks. Melanephelinite and high-Nb latitic minette plot as distinct rock types

elements (HFSE) (20–27 ppm Nb) in the Nb-rich lithology, these rocks display a negative Nb anomaly on a primitive mantle normalized trace element diagram (Figs. 7 and 8).

Clasts of the Nb-rich latitic minette are as large as 1 m in diameter with diameters of 20 cm and smaller being most common. Larger blocks commonly contain zones with readily apparent vesicles (and resulting lineation) and other areas that are vesicle free. The mica in the Nb-rich latitic minette is up to 8 mm in diameter, imparts a readily apparent flow foliation to the rock. Clinopyroxene phenocrysts are as large as 3 mm and lie in the diopside field (Fig. 5). Matrix feldspar in the Nb-rich latitic minette usually occurs as crystals smaller than 100 μm in both Nb-rich and Nb-poor varieties, and is nearly absent in some clasts. The feldspar crystals in the matrix are strongly zoned and consist of Ba-rich potassium feldspar, and, in a few instances, are found partially replacing (xenocrystic or intermixed?) plagioclase (Table 4). Large apatites are a common accessory phase. Titanium-in-biotite temperature of one sample is 1,047 ± 9 °C. Pressure estimates from Ba-contents average 3.8 ± 0.9 kb. Several types of inclusions are present

in the Nb-rich latite clasts. One type of inclusion is comprised dominantly of mica and clinopyroxene.

The Nb-rich latitic minettes have the highest incompatible element abundances found in any of the igneous rocks of the Bingham district. The trace element patterns are similar to the shoshonites (Fig. 7), just shifted upward. Despite the relative enrichment of Nb (20–27 ppm Nb) in these minettes, they still have negative Nb anomalies (Figs. 7 and 8). Negative Zr anomalies, seen in many evolved rocks, are not apparent in the latitic minette. Apparently, zircon crystallization was suppressed by relatively high temperatures and high alkali concentrations. Fractionation-induced enrichment of Zr causes these minettes to fall in the "within plate" fields (Fig. 12) on the discriminant diagrams of Müller and Groves (2000), even though they are clearly associated with and probably derived from arc-type magmatic rocks. Concentrations of Cu and PGEs are commensurately lower than in the shoshonites and melanephelinite, but the patterns are similar with strong enrichment of the more volatile elements (Fig 9).

Typical Nb-poor latitic minette (10–15 ppm Nb) occurs only as clasts in block and ash flows west of 112°6′. Clasts are gray-brown to light violet-brown and are usually 25 cm in diameter and smaller. Vesicles are less abundant in the Nb-poor latitic minette clasts than in Nb-rich latitic minette. The mica in Nb-poor latitic minettes (up to 20 modal%) is as large as 1.2 cm and also imparts a strong flow foliation. Even in completely unaltered samples, needles of exsolved rutile occur in subhedral to anhedral mica crystals, whereas euhedral phenocrysts contain only minor exsolution. Augitic clinopyroxene is also relatively abundant (up to 20 modal%) with crystals as large as 3 mm (Table 3). Small clinopyroxene crystals often occur around the edges of

Table 4 Representative major and trace element compositions of igneous rocks from the Bingham district. Major element in weight percent (wt%), Trace elements in parts per million (ppm). Most data collected by X-ray fluorescence spectrometry (XRF). Major elements normalized to 100% on a volatile-free methods and are measured in parts per billion (ppb). Major elements normalized to 100% on a volatile free basis. *Hybrid QMP* Hybrid quartz monzonite porphyry

	Rose Canyon						Bingham Deposit			
	Melanephelinite	Shoshonite		Latitic minette		Dacite	Minette	Biotite Porphyry	Hybrid QMP Rock	Enclave
				Nb-rich	Nb-poor					
	Tick-103	Lowe-21A	Tick-116	Tick-79	Tick-52A	Tick-83A	Bing-38	Bing-30A	Bing-45B	Bing-45A
SiO_2 wt%	44.50	53.62	55.71	58.67	59.03	67.97	57.85	62.21	67.25	59.64
TiO_2	0.96	0.84	0.75	1.08	0.93	0.50	0.66	0.54	0.62	0.93
Al_2O_3	10.20	12.52	12.78	14.14	13.63	15.12	12.96	13.98	15.82	13.50
Fe_2O_3	10.73	8.97	7.36	6.01	7.54	3.52	10.83	5.65	3.30	7.66
MnO	0.19	0.11	0.19	0.08	0.1	0.02	0.04	0.01	0.01	0.02
MgO	15.58	8.04	7.78	3.99	4.64	1.42	8.65	5.96	3.32	9.03
CaO	10.21	9.18	8.72	6.28	5.51	3.11	1.16	1.01	1.59	1.72
Na_2O	4.06	3.00	2.99	3.02	2.61	4.27	1.11	1.64	2.45	0.46
K_2O	2.87	3.22	3.34	5.93	5.28	3.83	5.88	8.25	5.28	6.63
P_2O_5	0.38	0.42	0.35	0.73	0.63	0.21	0.70	0.54	0.25	0.32
F O	0.31	0.08	0.03	0.07	0.1	0.03	0.15	0.20	0.11	0.08
SUM	100	100.00	100.00	100.00	100.00	100.00	100.00	100.00	100.00	100.00
LOI	1.36	1.32	2.45	1.16	1.44	0.48	3.60	2.84	1.82	3.15
Total	99.49	99.79	99.92	100.04	99.97	99.23	97.35	99.35	98.04	100.03
F ppm	5,700	1,800	600	1,700	2,300	700	3,600	4,800	2,400	4,200
S	100	0	0	0	0	0	4,100	4,900	6,100	6,100
Cl	100	100	200	200	400	100	1,000	300	100	300
Sc	25	23	19	16	14	7	16	11	7	24
V	201	169	127	79	147	40	159	123	82	163
Cr	955	624	646	163	89	68	353	275	66	473
Ni	354	97	345	91	27	39	472	267	59	157
Cu	126	35	65	25	49	14	3,200	10,300	6,300	7,000
Zn	99	53	71	71	74	37	–	–	–	–
Ga	12	16	17	19	18	20	17	17	20	22
As	2	<2	4	5	<2	3	–	–	13	2
Rb	79	75	86	160	163	117	342	290	170	301
Sr	1,117	642	708	1,350	866	819	46	154	529	202
Y	23	20	19	23	24	13	13	9	16	9
Zr	135	149	187	425	258	203	184	159	204	164
Nb	27	13	10	27	13	11	14	15	1	10
Mo[a]	1	1	–	1	<1	–	–	–	6	3
Ag[a]	0.2	0.2	–	<0.2	<0.2	–	–	–	–	–
Sb[a]	<2	<2	–	<2	<2	–	–	–	–	–
Ba	2,107	1,875	1,800	3,632	3,634	2,089	809	965	1,601	767
La	69	59	67	202	73	62	46	41	66	57
Ce	110	96	114	303	129	124	111	92	132	135
Pr[a]	14.2	11.1	–	31.8	16	–	16.1	–	15.5	–
Nd	54	43	54	117	55	45	47	37	50	49
Sm	8	7	10	20	8	9	9	8	9	9
Eu[a]	1.9	1.6	–	3.6	2.5	–	–	–	4.6	–
Gd[a]	7.2	5.7	–	13	8.2	–	–	–	5.8	–
Tb[a]	1	0.8	–	1.6	1.2	–	–	–	0.8	–
Dy[a]	4.6	3.5	–	5.8	5.1	–	–	–	3.2	–
Ho[a]	1	0.7	–	1.1	1	–	–	–	0.6	–
Er[a]	2.4	1.9	–	2.5	2.4	–	–	–	1.4	–
Tm[a]	0.4	0.3	–	0.3	0.4	–	–	–	0.2	–
Yb[a]	2.4	1.7	–	2.3	2.3	–	–	–	1.6	–
Lu[a]	0.4	0.3	–	0.3	0.4	–	–	–	0.3	–
Au[b]	<5	<5	–	<5	20	–	–	–	–	–
Hg[a]	<1	<1	–	<1	<1	–	–	–	–	–
Pb	11	19	28	64	49	41	5	7	16	10
Bi[a]	<2	<2	–	<2	<2	–	–	–	–	–
Th	8	12	17	40	21	19	29	21	49	11
U	4	4	5	9	7	4	8	7	9	10

[a] Data collected by inductively coupled plasma mass spectrometry (ICP-MS)
[b] Gold abundances were collected by fire assay and atomic absorption methods and are measured in parts per billion (ppb)
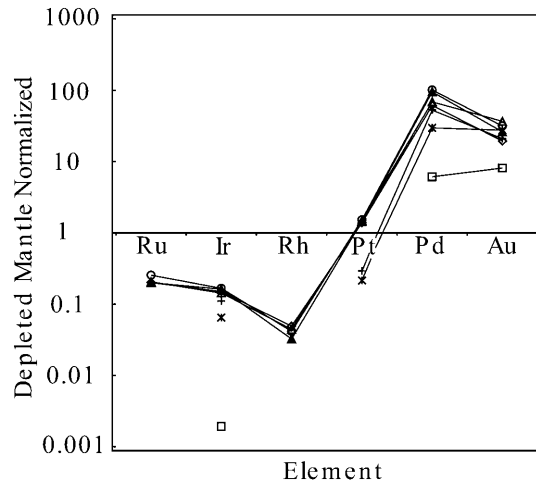
Fig. 9 PGE and Au abundances from Bingham district lava flows and block and ash flows normalized to depleted mantle (Evans et al. 1993)

the larger mica phenocrysts and may have partially replaced the mica (as a consequence of degassing). The average biotite temperature of one sample was $1,056 \pm 9$ °C, indistinguishable from that of the Nb-rich variety. Pressure estimates from Ba-contents of biotite (Righter and Carmichael 1996) in this sample range widely, but average 5.8 ± 3 kb. The Nb-poor latitic minettes have trace element patterns that are similar to the Nb-rich minettes, but are not as extreme (Fig. 7). They also have lower Ca, Al, and Sr.

Initial $^{87}Sr/^{86}Sr$ ratios are high for both rock types, 0.7108 for the Nb-rich latitic minette and 0.7134 to 0.7156 for the Nb-poor latitic minette. ϵNd (38 Ma) values of –20.6 were determined for the Nb-rich latitic minette and –18.4 to –20.0 for the two Nb-poor latitic minette clasts. These ϵNd values are among the lowest found in the Bingham district (Fig. 10, Table 6). Nd model ages range from 1.4 to 1.9 Ga.

Trachyte and dacite clasts in block and ash flow

The bulk of the clasts in the block and ash flows of Rose Canyon straddle the border between trachyte and dacite (Fig. 3), and typically have phenocrysts of amphibole, plagioclase, and in some samples, clinopyroxene and biotite. A few clasts in block and ash flow have mafic cumulate(?) inclusions as large as 5 cm across that are rich in amphibole, biotite, clinopyroxene, Fe–Ti oxides and less commonly olivine. Chrome abundances of these enclaves are as high as 2,000 ppm, Ni as high as

310 ppm, and SiO_2 contents range from 45 to 54 wt%. Pulsipher (2000) and Waite et al. (1997) describe in more detail the characteristics of trachyte and dacite clasts. These silicic rocks have relatively high Mg/Fe ratios (making them calc-alkaline), high oxygen fugacities ($\Delta NNO > 2$), medium to high K_2O contents, and trace element patterns and variation trends typical of continental arc, calc-alkaline volcanic rocks. Initial $^{87}Sr/^{86}Sr$ of two dacites are lower than the olivine latites and latitic minettes, but ϵNd (38 Ma) is low like the others (Fig. 10) suggesting that they were produced by the same set of complex mafic recharge, fractionation, and crustal contamination that created the other volcanic rocks. This "older series" differs from the younger, post-mineralization volcanic rocks at Bingham by their higher concentrations of Cr and Cu at comparable SiO_2 contents.

Intermediate dikes/plugs of Rose Canyon

A few small intrusions between 5 and 100 m wide, with intermediate compositions of 59–66 wt% SiO_2 crosscut some of the youngest exposures of the block and ash flows in Rose Canyon (Fig. 4). All the intrusions have amphibole phenocrysts up to 1.5 cm in diameter, biotite as large as 1 cm, and clinopyroxene as large as 3 mm. Plagioclase occurs as rare crystals in the matrix of the more mafic samples and as small phenocrysts in the most siliceous. Pulsipher (2000) classified those dikes that lack feldspar phenocrysts as spessartite lamprophyres following the IUGS classification of lamprophyres (Rock 1991).

Mafic to intermediate alkaline intrusions of the Bingham system

The main Bingham intrusions have ages ranging from 39.8 to 37.5 Ma (Warnaars et al. 1978). Potassic, phyllic, and other types of alteration have overprinted and significantly altered the original magmatic mineralogy and chemistry. Bingham mineralization is overprinted on monzonite, quartz monzonite porphyry, quartz latite porphyry, latite porphyry, and quartz latite porphyry breccia. These units will not be addressed in this paper and have been more extensively studied or reviewed by others (Lanier et al. 1978a; Babcock et al. 1997; Phillips et al. 1997; Pulsipher 2000; Redmond and Einaudi 2000). Pulsipher (2000) tabulates chemical and mineralogical similarities between these intrusions and the clasts in block and ash flows of Rose Canyon and concludes that they are co-magmatic. However, other coeval alkaline intrusions hosted by the Bingham stock that have not been studied as extensively by other workers are described in this paper.

Minette dikes

Two minette dikes are present on about the 6,090′ level of the northwest side of the Bingham open pit. Such

Table 5 PGE and Au abundances of selected samples from the Bingham district compared with abundances of samples from Figi and Lihir. *bld* Below detection limit

Location	Sample	Pd (ppb)	Pt (ppb)	Au (ppb)	Ir (ppb)	Ru (ppb)	Rh (ppb)
Bingham	Melanephelinite (Tick-38)	8.56	6.27	1.0	0.312	0.28	0.15
Bingham	Melanephelinite (Tick-39)	6.20	6.44	1.5	0.276	0.29	0.20
Bingham	Melanephelinite (Tick-43)	5.52	5.97	0.8	0.289	0.29	0.23
Bingham	Melanephelinite (Tick-44)	9.08	6.59	1.3	0.321	0.36	0.19
Bingham	Melanephelinite (Tick-44)	10.0	9.24	2.3	0.499	0.38	0.18
Bingham	Nb-poor latitic minette (Tick-52A)	2.66	0.93	1.1	0.125	b.l.d.	b.l.d.
Bingham	Trachyte (Tick-59A)	0.55	bld	0.3	0.004	b.l.d.	b.l.d.
Bingham	Nb-rich latitic minette (Tick-66A)	4.73	1.27	0.8	0.212	b.l.d.	b.l.d.
Emperot, Fiji	136136	15.5	6.78	3.0	0.027	0.01	0.09
Emperor, Fiji	136147	11.3	3.42	2.3	0.038	0.00	0.02
Feni, PNG	136166	7.72	2.84	1.4	0.036	0.01	0.07
Lihir, PNG	136167	10.7	9.98	2.4	0.084	0.08	0.15
Lihir, PNG	45DR-1C	1.40	0.87	1.2	0.040	b.l.d.	b.l.d.
Detection limit (ppB)		0.01	0.36	0.1	0.003	0.01	0.01

dikes have not been previously mapped, probably because they are very narrow and do not naturally outcrop because of their mica-rich character. The dikes were located and sampled in 1996 with the assistance of Kennecott mine geologists. Neither dike is as veined as the host hybrid quartz monzonite porphyry and quartz latite porphyry, although both dikes contain significant Cu mineralization (up to 2,100 ppm Cu) and hydrothermal alteration. These dikes consist of 60 to 80 vol% biotite, which is largely magmatic. Some of the primary biotite phenocrysts are as large as 3 cm and are fractured and bent. These crystals impart a strong flow foliation to the rock parallel to the margin of the dike. The mica (phlogopite re-equilibrated to biotite) in one sample (Bing-40) has re-equilibrated to a Cr-poor composition despite the high Cr content of the rock (Table 2). Other large grains of mica sampled from the minette dikes of the Bingham pit have as much as 1.5 wt% Cr. The micas commonly have exsolved rutile. The large biotite phenocrysts are surrounded by hydrothermal alteration products: small shreddy biotite flakes, potassium feldspar, sparse apatite, and ~2% sulfides. Narrow quartz veins traverse the dikes. Despite the potassic alteration, which depleted Mg, Ca, Na, Ba, and Sr, the dikes retain a relatively mafic "immobile" trace element signature with 300 to 900 ppm Cr (Figs. 3 and 11) and high Sc, V, and Ni. High concentrations of relatively immobile incompatible elements (e.g., Zr, Nb, Ti, Ce, P, and Th) are also consistent with a minette protolith (Fig. 7, Table 4, Bing-38).

Some clots of alteration minerals have distinct mineral shapes suggesting pseudomorphs after olivine or pyroxene. One sample, Bing-38, has a $^{40}Ar/^{39}Ar$ step heating age of 37.74 ± 0.11 Ma (Deino and Keith 1997).

Biotite porphyry

Recent mapping of the Bingham deposit has revealed the existence of a 4–6-m wide, relatively mafic dike informally called biotite porphyry (Redmond and Einaudi 2000). Biotite porphyry phenocrysts consist of biotite and plagioclase. Biotite makes up about 12 vol% of the rock, occurs as subhedral to anhedral crystals as large as 0.5 cm, and contains exsolved crystals of rutile. Subhedral phenocrysts of plagioclase are mostly replaced by sericite and clay and are scalloped or embayed around the edges. Plagioclase phenocrysts as large as 4 mm make up about 1–5 vol% of the sample. Relict phenocrysts of amphibole, now completely replaced by shreddy biotite, are also present. The phenocrysts are set in a matrix of chlorite, biotite, quartz, sericite, apatite, sulfide, and clay. The biotite porphyry SiO_2 contents range from 59 to 62 wt%, and Cr contents range from 270 to 370 ppm. Biotite porphyry is the third of five mineralizing porphyry intrusions at Bingham and is less mineralized than the first two (Redmond and Einaudi 2000).

Hybrid quartz monzonite porphyry

Early mapping of the Bingham stock revealed that substantial outer portions of the quartz monzonite porphyry (QMP) were more mafic than the main interior mass of the intrusion. These portions were mapped as "hybrid QMP" and the inference was made that they were formed by "assimilation" of the earlier emplaced monzonite by the quartz monzonite porphyry (Lanier 1978a). Lanier (1978a) describes the contact between the QMP and the hybrid QMP as "abrupt". Prior to mining, the hybrid QMP occurred as two large rootless intrusions (up to 250 m wide as well as other smaller occurrences) on each end of the elongated and younger mineralized QMP intrusion. Most of the hybrid QMP has now been mined and only a small portion of one of the rootless intrusions remains. Both the QMP and the hybrid QMP are more porphyritic (finer-grained matrix) at higher elevations and more equigranular at deeper levels.

Phenocryst abundance is variable with ~ 20 vol% K-feldspar (up to 8 mm), ~10% quartz (1–2 mm), ~5–

Table 6 Strontium and Nd isotopic compositions of selected samples from the Bingham magmatic center. *HQMP* Hybrid quartz monzonite porphyry; *QLPD* quartz latite porphyry dike; *L Minette* latitic minette; *Tick-79* Nb-rich; *Tick-52A* and *Tick-52J* Nb-poor

Sample No.	Rock type	Rb (ppm)	Sr (ppm)	87Sr/86Sr (present)	(±)	87Rb/86Sr	87Sr/86Sr (t)	εSr (t)[a]	Nd (ppm)	Sm (ppm)	143Nd/144Nd (present)	(±)	εNd (present)	147Sm/144Nd	143Nd/144Nd (t)	εNd (t)	TDM (Ga)[b]
Bing-6	Latite	122	741	0.711425	22	0.4752	0.711169	92	47.1	7.58	0.511722	14	−17.9	0.0973	0.511698	−17.4	1.7
Bing-17	QLPD	164.3	1066	0.708591	16	0.4758	0.708334	51	58.10	8.64	0.511683	10	−18.6	0.0899	0.511611	−18.1	1.7
Bing-19	Monzonite	121.7	1349	0.708319	21	0.2610	0.708178	49	64.7	9.99	0.511606	18	−20.1	0.0932	0.511582	−19.6	1.8
Bing-23	QLPD	118	763	0.708065	12	0.4461	0.707824	44	47.11	7.73	0.511825	12	−15.8	0.0991	0.511801	−15.4	1.6
Bing-45B	HQMP	159	553	0.709087	12	0.8279	0.708640	56	35.18	5.42	0.511748	18	−17.4	0.0932	0.511725	−16.9	1.6
Bing-51	Latite dike	190	1057	0.711837	22	0.5210	0.711556	97	54.13	8.65	0.511596	12	−20.3	0.0966	0.511572	−19.8	1.8
Bing-53	Latite dike	106	727	0.711771	28	0.4244	0.711542	97	45.82	7.57	0.511669	18	−18.9	0.0999	0.511644	−18.4	1.8
BM-2	QLPD	98.6	882	0.707655	10	0.3235	0.707480	39	43.66	6.76	0.511640	18	−19.5	0.0936	0.511617	−19.0	1.8
Lowe-21A	Shoshonite	90.1	684	0.708841	12	0.3815	0.708635	56	38.16	6.66	0.511790	12	−16.6	0.1054	0.511764	−16.1	1.7
5090-600	QMP	164	583	0.708886	12	0.8148	0.708446	53	27.35	4.23	0.511676	10	−18.8	0.0934	0.511676	−18.3	1.7
Tick-16	Latite	84.7	1506	0.707558	14	0.1627	0.707484	39	73.84	10.49	0.512034	12	−11.3	0.0858	0.512016	−11.3	1.1
Tick-40	Dacite	124	541	0.708297	10	0.6655	0.707995	47	40.78	6.02	0.511775	10	−16.4	0.0892	0.511756	−16.4	1.5
Tick-42	Rhyolite	99.3	722	0.709142	12	0.3976	0.708961	61	44.36	7.97	0.511774	14	−16.5	0.1086	0.511751	−16.5	1.8
Tick-43	Melanephelinite	61.3	445	0.707057	17	0.3984	0.706842	30	24.1	4.04	0.512210	18	−8.3	0.1013	0.512185	−7.9	1.1
Tick-44	Melanephelinite	94.5	1492	0.707238	10	0.1833	0.707139	35	45.50	7.53	0.512259	8	−7.4	0.1000	0.512234	−6.9	1.1
Tick-44A	Olivine latite	125	815	0.711931	21	0.4450	0.711691	99	50.9	8.74	0.511726	28	−17.8	0.1037	0.511700	−17.3	1.8
Tick-46	Olivine latite	144	841	0.712860	16	0.4953	0.712593	112	47.63	8.32	0.511624	18	−19.8	0.1055	0.511598	−19.3	1.9
Tick-52A	L minette	164	1388	0.713554	16	0.3330	0.713374	123	54.64	5.13	0.511579	8	−20.7	0.0567	0.511565	−20.0	1.4
Tick-52J	L minette	186	1001	0.715868	24	0.5375	0.715578	154	56.68	9.99	0.511670	14	−18.9	0.1065	0.511644	−18.4	1.9
Tick-55A	Latite	64.3	980	0.710276	36	0.1898	0.710174	78	62.2	10.02	0.511695	8	−18.4	0.0973	0.511671	−17.9	1.7
Tick-55I	Dacite	114	926	0.711616	22	0.4011	0.711400	95	39.6	5.79	0.511595	15	−20.3	0.0884	0.511573	−19.8	1.7
Tick-79	L minette	181	1624	0.710966	14	0.3231	0.710792	86	112.6	18.13	0.511556	14	−21.1	0.0974	0.511532	−20.6	1.9
Tick-82	Dacite	122	831	0.711511	36	0.4260	0.711281	93	35.93	5.59	0.511563	14	−21.0	0.0940	0.511540	−20.5	1.8
Tick-103	Melanephelinite	89.9	1542	0.706886	32	0.1695	0.706795	30	52.99	8.92	0.512261	18	−7.4	0.1018	0.512236	−6.9	1.1

[a] Calculated at t = 38 Ma (or t = 32 Ma for Tick 16, Tick 40, Tick 42) based on the present values of $^{87}Sr/^{86}Sr = 0.704755$ and $^{87}Rb/^{86}Sr = 0.08923$ (Allegre et al. 1983)

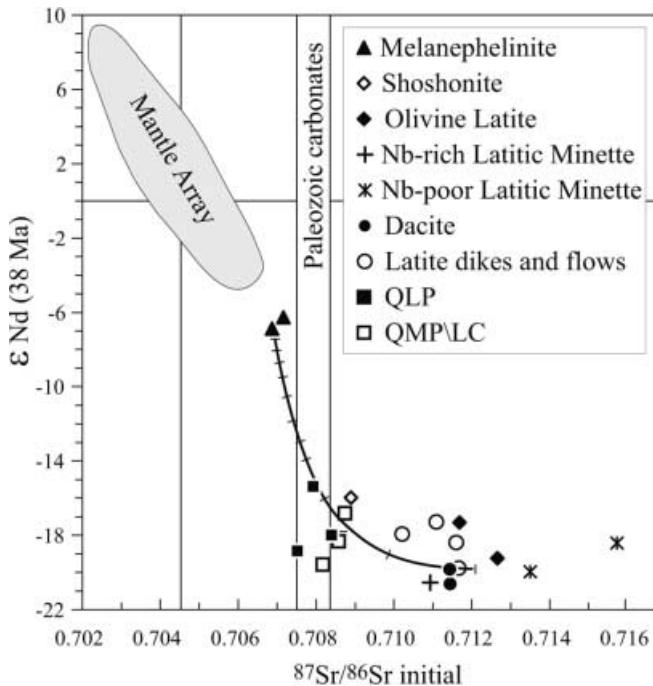[b] T_{DM} depleted mantle model age based on Michard et al. 1985

Fig. 10 Initial Sr and Nd isotope ratios for volcanic and intrusive rocks from the Bingham district. The *shaded region* shows the composition of mantle-derived rocks from ocean basins. The *vertical band* shows the composition of the carbonate wall rocks of the intrusion with the implication that post-magmatic alteration may have altered the Sr isotopic composition of the intrusions. A simple mixing curve illustrates the effect of mixing a mafic alkaline magma (with 1,200 ppm Sr and 50 ppm Nd) with an evolved magma (with 200 ppm Sr and 45 ppm Nd) with high $^{87}Sr/^{86}Sr$ and low ϵNd. The mixing array falls near the composition of the intrusive rocks (QMP, QLP, and LC). *Tick marks* show increments of 10%

10% plagioclase, and ∼5–8% biotite (up to 5 mm). Biotite crystals have strong pleochroism, exsolved needles of rutile as inclusions on cleavage planes, and are subhedral to anhedral. Typical hybrid QMP has 67–68 wt% SiO_2 and 60–70 ppm Cr which is only slightly higher than ordinary QMP (Fig. 3, Table 4). Compatible trace elements are present in higher concentrations in the hybrid QMP than in either the QMP or the host monzonite that supposedly was assimilated. For example, the adjacent intrusions of quartz monzonite porphyry and monzonite typically have between 35 and 60 ppm Cr. Initial $^{87}Sr/^{86}Sr$ ratios for QMP and hybrid QMP are similar (0.7085 versus 0.7087), but hybrid QMP shows a slightly less negative ϵNd (38 Ma) isotopic value of –16.9 compared with –18.3 for the QMP (Table 6).

Mafic inclusions are commonly found in the hybrid QMP and are one criterion used by Kennecott mine geologists to distinguish hybrid QMP from normal QMP. One inclusion (associated with Bing-45B) has about 20 vol% phenocrystic biotite, 59.6 wt% SiO_2 and 470 ppm Cr (Table 4; Bing-45A). These inclusions appear to indicate that the parental monzonitic magma of the hybrid QMP may have mixed with a more mafic component during or prior to intrusion rather than assimilating large volumes of adjacent rock at epizonal levels. Petrographic evidence of mixing, if once present, was obscured by mineralization.

Discussion

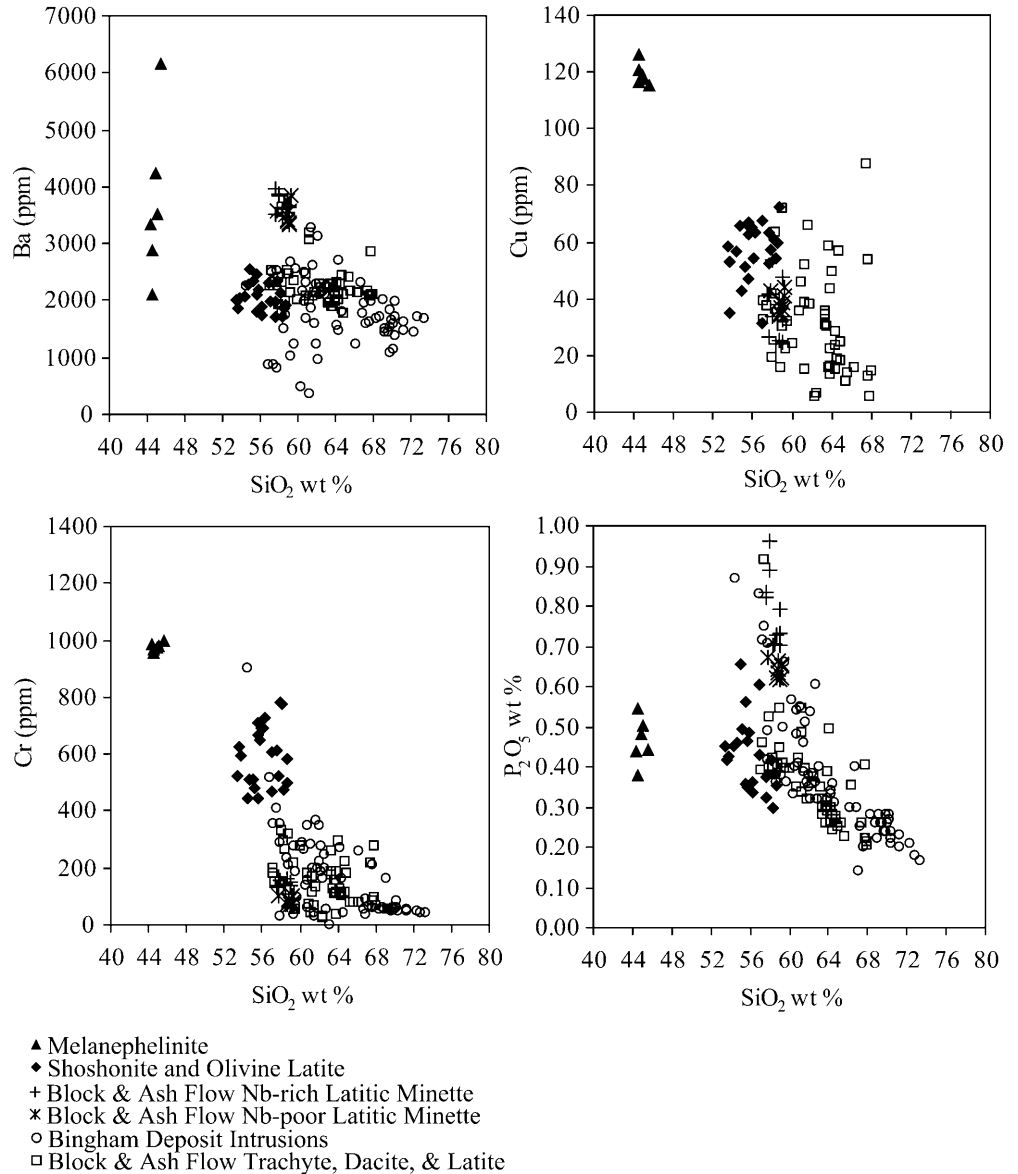Petrogenesis of alkaline igneous rocks in the Bingham district

The origin of the mafic alkaline magmas of the Bingham district reflects the tectonic history of western North America. Jurassic to early Tertiary orogenic episodes of western North America indicate episodically compressional to transtensional environments. During the early Cenozoic, the Farallon Plate subducted at a very low angle under the North American Plate (Armstrong et al. 1969; Severinghaus and Atwater 1990). During the late Eocene, the Farallon Plate appears to have detached from the lithosphere in a southward sweeping motion allowing hot asthenospheric mantle to flow between the subducting slab and the relatively colder lithospheric mantle (Best and Christiansen 1991). At about the same time, we speculate that small amounts of extension, crustal thinning, and mild decompression may have occurred in northern Utah and are manifest by mineralized N50°E-trending faults in and around the Bingham deposit. The heating of the lithospheric mantle with hot asthenospheric mantle, subduction and dewatering of the Farallon Plate, and decompression of hot lithospheric mantle associated with minor extension are all probably responsible to various degrees for small amounts of partial melting of the lithospheric and asthenospheric mantle.

In the sections that follow, we first consider whether the melanephelinite flows in the Bingham district are primary magmas and then speculate about the nature of their sources and relationships with other magmatic rocks in the district.

Melanephelinite

The melanephelinite of Rose Canyon is the most mafic and primitive of any lava known to occur in the Bingham district. Phenocrysts of Fo_{91}–Fo_{87} (some of which are intergrown with phlogopite), high Mg/Fe ratios, and high concentrations of compatible elements (e.g., 950–1,000 ppm Cr, and ∼350 ppm Ni; Fig. 11, Table 4) indicate these magmas were primitive and formed in equilibrium with mantle peridotite and suggest little differentiation or contamination of the magma. If this is the case, the mantle source must have been metasomatized to produce the arc-like platinum group element and incompatible trace element patterns (Figs. 8 and 9). These are unlike the OIB-like patterns found in other continental melanephelinites associated with the Late Tertiary extension (Tingey et al. 1991). Some high field

Fig. 11 Variation diagrams for Bingham district rocks. Copper concentrations for samples from the Bingham pit are not included as they contain up to 2 wt% Cu

▲ Melanephelinite
◆ Shoshonite and Olivine Latite
+ Block & Ash Flow Nb-rich Latitic Minette
✳ Block & Ash Flow Nb-poor Latitic Minette
○ Bingham Deposit Intrusions
□ Block & Ash Flow Trachyte, Dacite, & Latite

strength elements (e.g., Ti, Zr, and Nb; Fig. 7) have abundances higher than typical mafic arc magmas, but large ion lithophile elements (LILE) are extremely enriched (~95 ppm Rb, 700–1,600 ppm Sr, and 2,000–6,000 ppm Ba; Fig. 11) for a primitive magma. Small degrees of partial melting of the lithospheric mantle bearing amphibole and phlogopite could generate melts enriched in LILE and depleted in Nb and Ti. The consistently sodic character ($Na_2O > K_2O$) of the melanephelinites may be the result of derivation from amphibole peridotite (Francis and Ludden 1995). However, the Bingham melanephelinites have higher K_2O, Rb, and Ba and lower TiO_2 than typical melanephelinites – perhaps as a result of phlogopite in their mantle source as well. The shallow slopes of the REE patterns severely limit the amount of residual garnet in the source. Residual apatite is indicated by small negative phosphorous anomalies on normalized trace element diagrams. However, none of

the melanephelinites have phenocrysts of apatite; MELTS (Ghiorso and Sack 1995) calculations also show that apatite crystallizes only at temperatures below 1,050 °C. The high contents of Cu, PGE, Au, and S were probably established at the source by melting sulfides in metasomatized lithospheric mantle. Likewise, high oxygen fugacities may be characteristic of this type of metasomatized mantle (Carmichael 1991).

It is unlikely that even extremely small degrees of partial melting of convecting depleted asthenosphere, similar to that which gives rise to ocean island basalts, produced these alkaline magmas. These alkaline rocks bear a strong subduction-zone imprint as the result of melting of anciently enriched lithospheric mantle as evidenced by their very low εNd values. They probably formed by a larger degree of partial melting of enriched lithospheric mantle. Generalized batch partial melting calculations using a metasomatized high-K peridotite of
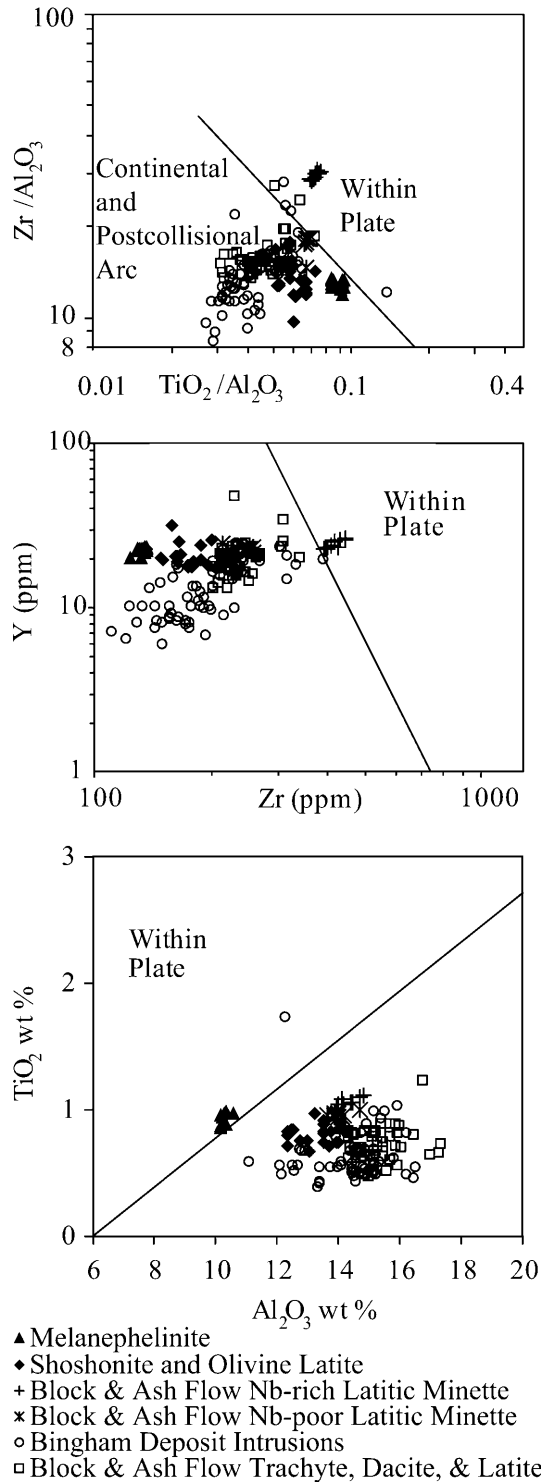
Fig. 12 Tectonic discrimination diagrams (Müller and Groves 1993, 2000) for rocks from the Bingham district. Sometimes melanephelinite and Nb-rich latitic minettes show "within-plate" affinities. Other volcanic and intrusive units are overwhelmingly arc-related

Hartmann and Wedepohl (1990) show that about 5% melting can produce the enrichments of many incompatible trace elements found in the melanephelinite.

However, depletions of Th, Nb, and Ti are not produced without assuming distinctive minerals (phlogopite, amphibole, apatite, and titanates) were residual. Light rare earth elements are enriched (~70 ppm La and ~105 ppm Ce) relative to chondrite values uncharacteristic of a depleted mantle source (Fig. 8, Table 4). Indeed, $^{87}Sr/^{86}Sr$ ratios (0.7068–0.7071) are very high and ϵNd (38 Ma) are low (–6.9; Table 6) and fall off the "mantle array" defined by oceanic rocks. These isotopic compositions show that the melanephelinite source was enriched in incompatible elements for a long time (Table 6). Nd model ages for the melanephelinite are 1.1 Ga, but the assumption that the Sm/Nd ratio was unchanged during partial melting is probably not valid for such low degree melts; a lower Sm/Nd ratio in the melt compared with its source would make the model age younger than the actual age of the source. The role of crustal contamination in the melanephelinites is difficult to constrain, but their primitive character suggests it might have been unimportant.

In short, we interpret the Bingham melanephelinite to be a partial melt of a hydrous, oxidized, sulfur-, base- and precious metal-enriched, metasomatized mantle. This metasome conceivably was heterogeneously distributed as veins or pods in the lithospheric mantle. Enrichment of large ion lithophile elements may have occurred during slab dehydration or by the introduction of melts from the mantle wedge, but much of the enrichment was ancient and probably occurred during initial formation of this part of the lithosphere sometime in middle Proterozoic time.

Mixing of the silica-undersaturated component into already existing calc-alkaline, subvolcanic magma chambers could have added significantly to the overall budget of water, sulfur, and ore metals in evolving silicic magmas that eventually gave rise to the Bingham ore deposit. The overall high concentrations of compatible elements such as Cr and Ni that occur in the relatively more siliceous rock units of Bingham are consistent with this process (Waite et al. 1997; Fig. 11).

Olivine latite and shoshonite

High concentrations of compatible elements in some of the shoshonites and olivine latites require evaluation of their potentially primary nature as well. Judging from traditional tests for equilibrium with mantle peridotite, these magmas were probably not primary. The shoshonites have mg# up to 0.70, but have too little Ni (less than 150 ppm) and Cr (less than 700 ppm) to have formed in equilibrium with peridotite. Likewise, the high SiO_2 contents of the olivine latites also suggest that they are not primary. In spite of high Ni concentrations, these rocks all have MgO less than 8 wt% and MgO/Ni ratios that are inconsistent with equilibration with normal peridotite. The high mg# and relatively forsteritic olivines of both rock types are more likely the result of crystallization at high f_{O_2} than of direct derivation from

the mantle. As a result, the interpretation of their isotopic ratios as being derived from enriched lithospheric mantle is not straight-forward. In fact, the distinctive major and trace element compositions of the olivine latites, along with petrographic, mineralogic, and field evidence reveal that they formed by crustal contamination of melanephelinite, probably at a very shallow, subvolcanic level. The olivine latites have extremely high concentrations of mantle compatible trace elements (Fig. 11), especially Ni, Cr, and Cu, for their intermediate compositions. Mixing of melanephelinite magma with more silicic calc-alkaline magmas (as speculated by Waite et al. 1997) is inconsistent with their relatively low Ba contents and their Zr and Nb concentrations (Fig. 8). Instead, assimilation of (impure?) quartzite combined with fractionation of olivine and/or clinopyroxene explains many of their geochemical characteristics as well as their enriched isotopic compositions (Fig. 10). The pyroxene inclusions may be products of this process. According to MELTS calculations (Ghiorso and Sack 1995), progressive assimilation of 10% quartzite into the silica-undersaturated melanephelinite results in crystallization of olivine as the sole silicate phase over an interval of about 100 °C. If a higher proportion of assimilation is assumed, as the melt becomes more contaminated and fractionated, olivine ceases to crystallize and clinopyroxene alone fractionates. Such complicated crystallization histories may be consistent with the scatter of olivine latites on compatible versus incompatible element diagrams.

The most common shoshonites also have characteristics that link them to the melanephelinites through magma mixing processes. Major element models and isotopic ratios suggest that these shoshonites could have formed by mixing melanephelinite with trachyte (in 5:3 proportions) in conjunction with fractionation of about 15% olivine and assimilation of about 10% of quartzite and less than 1% carbonate wallrocks.

Fractionation of shoshonite to form latitic minette

Geochemical relationships show that the shoshonites could have fractionated to form latitic minette. In many ways, the latitic minettes are the most fractionated rocks found in the Bingham district. Enrichment factors for incompatible elements suggest that a parental shoshonite must have experienced about 40% crystallization to reach the Th, Zr, Nb, LREE, P, Ba, Sr, K, and Ti enrichments found in the Nb-poor latitic minettes (Fig. 7). MELTS calculations (Ghiorso and Sack 1995) and major element mass balance models suggest about 35 to 60% crystallization of olivine and clinopyroxene (with or without assimilation of sedimentary wall rocks), from a parental shoshonite could produce the Nb-poor latitic minettes. Isotopic ratios require assimilation of wall rocks. The fractionated mineral assemblages must have been dominated by clinopyroxene to explain the drop in CaO and CaO/Al$_2$O$_3$ ratio with increasing SiO$_2$. Lesser

olivine and little or no apatite and feldspar were removed as indicated by the absence of P and Sr anomalies on the trace element diagrams (Fig. 7). Strong Rb and Ba enrichments (Fig. 11, Table 4) suggest that phlogopite crystallization occurred late in the fractionation sequence. As fractionation proceeded, water and potassium concentrations increased to the point that phlogopite was stabilized at the expense of olivine. High water contents probably retarded the crystallization of feldspar (Blatter and Carmichael 1998). Low concentrations of Cu and PGEs are probably the result of the removal of magmatic sulfide blebs.

On the other hand, we have found no satisfactory major or trace element model that relates the shoshonites to the Nb-rich latitic minettes. Incompatible elements require 60 to 70% crystallization of shoshonite, but the compatible elements (e.g., Ni and Cr) are not strongly depleted as predicted by this model. The Nb-rich latitic minette may not be directly derived from any of the sampled shoshonites or melanephelinite of the Bingham district.

The high initial ^{87}Sr/^{86}Sr ratios (0.711–0.715) and low ϵNd (38 Ma) (–18 to –21) of the latitic minettes are consistent with significant assimilation of upper crustal materials during fractionation and probably reveal little about the composition of lithospheric mantle.

Latitic minette may have not been directly involved with mineralization of the Bingham stock. Nonetheless, these highly fractionated magmas may have intermingled with other contemporaneous magmas in subvolcanic chambers. Evidence for mingling is in the form of scatter in the composition of some dacite and trachyte clasts in the block and ash flow toward the distinctive composition of the Nb-rich latitic minette on variation diagrams. A wide variety of elements show this pattern, including large ion lithophiles, high field strength, and compatible elements (e.g., Sr, Ba, Rb, K, P, Ti, Zr, Nb, Y, Sc, and Ni). Plagioclases of dacite and trachyte clasts are strongly zoned and typically resorbed or sieved, consistent with mixing.

Tectonic setting

The preceding data indicate that multiple magmas with components from several different mantle sources were likely fractionated, contaminated, and co-mingled during the life span of the Bingham magmatic system. Melanephelinite lavas did not appear until relatively late in the Bingham-related eruptive sequence. On the tectonic discrimination diagrams of Müller and Groves (2000) for potassic igneous rocks, the melanephelinite (while not strictly speaking potassic) generally falls within the "continental arc" field, but its low Al$_2$O$_3$ concentrations give it a "within plate" affinity.

Consequently, could some change in tectonic setting have occurred during the relative short life span of this volcano and affected the production and delivery of batches of magma?

Identifying subtle changes in the state of stress for this area at 38 Ma may be difficult. However, what is clear is that the nature and morphology of intrusions changed dramatically with time. The initial intrusion of monzonite of the Bingham stock and the Last Chance stock shows no preferred orientation of intrusion (Fig. 2; Lanier et al. 1978a) and did not produce any mineralizing fluids. By contrast, all subsequent intrusions into the Bingham stock are dike-like, trending approximately N50°E, and are related to mineralization. The Last Chance and Bingham stocks were emplaced by stoping whereas subsequent intrusions were forcefully emplaced. We find little or no evidence that the amphibole-free, equigranular monzonite of the Last Chance and Bingham stocks vented to the surface, whereas subsequent Bingham magmas did. The trend towards forceful dike-like intrusions, late in the history of this volcano, may have allowed delivery of primitive sulfur- and water-rich magmas to the base of the magma chamber at the time of ore formation. This unique magma may have originated as a small degree melt of the lithospheric mantle as a result of a small amount of extension in conjunction with heat derived from subduction-zone magmatism. An asthenospheric source for the melanephelinite is possible, but its trace element pattern is characteristic of arc-magmas. Certainly, a composite source from both asthenospheric and lithospheric magmas would account for the unique ϵNd signature of this magma (much higher than other Bingham magmas).

Sulfur- and water-rich magmas

Several lines of evidence indicate that the melanephelinite magma was water- and sulfur-rich prior to eruption. The water content of the melt is unknown, but was probably high. Fresh rocks contain 1–3 wt% H_2O and this is probably a lower limit on the magmatic concentration because of degassing before and after eruption. The presence of primary mica phenocrysts and abundant mica in the groundmass show that magmatic water content must have been high. MELTS calculations show that at least 2% water is needed to stabilize phlogopite over leucite. The experiments of Esperanca and Holloway (1987) and Righter and Carmichael (1996) with minettes similar except for their high K/Na ratios, show that in excess of 4% water must have been dissolved in the melt. Sulfur solubility is generally positively correlated with Fe content and f_{O2} of the magma. Although the original sulfur content of the melanephelinite magma is not known, it was likely to be high based on the presence of barite inclusions in olivine, high Fe content (>10 wt% total Fe as Fe_2O_3; Table 4), and high oxidation state (log $f_{O_2} = NNO + 2.5$; Tomlinson et al. 2000). Hattori and Keith (2001) cite data from analogous systems that primitive subduction zone melts or mafic alkaline melts may commonly have over 3,000 ppm sulfur. Regardless of the exact origin of the

barite inclusions, they may indicate that the magma was more sulfur-rich than the final consolidated rock that has less than about 400 ppm sulfur. It is not unreasonable that over 90% of the magmatic sulfur was lost by degassing upon eruption or in subvolcanic magma chambers (Larocque et al. 2000; Hattori and Keith 2001).

Co-mingling of mafic and silicic magmas

What evidence exists that mafic magmas participated in formation of the ore-related intrusions or ore-related fluids? The following observations should be cited in this regard:

1. The mafic character of the hybrid quartz monzonite porphyry (especially including the numerous mafic clots) is unlikely to be explained by assimilation of neighboring more evolved intrusions, but rather by magma mixing involving a mafic alkaline magma and a quartz-bearing calc-alkaline magma.
2. The presence in breadcrust-textured dacite of mafic clots comprised of amphibole rimming clinopyroxene, biotite, and iddingsite after olivine (Keith et al. 1998; Pulsipher 2000).
3. The elevated Cr and Ni content of all of the ore-related Bingham intrusions coupled with the trend of the younger Bingham intrusions to be more Cr- and Ni-rich despite their otherwise more evolved geochemical signatures (Waite et al. 1997; Pulsipher 2000).
4. The Pd- and Pt-rich character of the Bingham ore coupled with the Pd- and Pt-rich signature of the melanephelinite (Fig. 9, Table 5). This enrichment of Pd, Pt (and Au) relative to other platinum group metals is similar to that seen in other young shoshonitic alkalic systems like those of Fiji and Lihir, Papua New Guinea (Table 5; and Müller et al., in preparation).
5. Shoshonitic and latitic scoria co-erupted with quartz- and sapphire-bearing dacite/trachyte pumice and ash at the approximate time of ore formation (Pulsipher 2000).

Other correlations can be drawn that connect the volcanic deposits with the evolving Bingham magmas, but the above points emphasize that mafic magmas actually mixed with the silicic magmas at the approximate time of ore formation.

Contributions of sulfur and metals
from mafic magmas

Although giant porphyry copper deposits, such as Bingham, are noted for the extreme tonnages of copper, gold, and other metals they contain (over 3 billion tons of ore at 0.73% Cu and more than 40 million ounces of

gold; Ballantyne et al. 1997), these data are dwarfed by the total amount of sulfur in the deposit. Gustafson (1979) noted that "sulphur is genetically, if not economically, a more important factor than the metals [in formation of porphyry copper deposits]... Hunt (1977) pointed out, porphyry copper deposits are really large sulphur anomalies with lower Cu/S ratios than ordinary crustal rocks." Magmatic sulfur enrichment may be the critical process that ultimately leads to porphyry-type ore formation; copper and other metals may "just go along for the ride" and show less relative enrichment in the final ore deposit (Keith et al. 1999).

For example, mass balance calculations that estimate the amount of magma that would need to be stripped of metals to account for the metal typical in porphyry deposits yield magma volumes in the range of 50 to 200 km^3 assuming average Cu or Mo concentrations in the ore-related granitoids (Keith and Christiansen 1992; Dilles and Proffet 1995). However, if average magmatic S concentrations ($\sim$100 ppm) are used to make the same estimates for Bingham, then at least 3,500 km^3 of felsic magma would be required (Hattori and Keith 2001). What is the answer to this incongruity? If prior to ore formation the dacitic magma at Bingham was enriched in S to levels comparable with those noted for Mount Pinatubo (around 2,000 ppm), then 100–200 km^3 of magma would be sufficient for a S source as well. These high concentrations at Mount Pinatubo were likely achieved by underplating and injection of basaltic magma (Hattori 1993) and transfer of S-rich fluids into the overlying dacitic magma chamber.

Clearly, if intermediate composition magmas become enriched in sulfur by this process and then both the magma and sulfur are erupted, that sulfur will be dispersed and never form a deposit. However, during the life span of a single volcano, the magma chamber may be recharged and underplated repeatedly. During the waning stages of the volcano, some batches of magma may become sufficiently crystal-rich that they become too viscous to erupt, despite having accumulated excess sulfur. If the process of "enriching" the cupola magma with excess sulfur operates regardless of the ultimate fate of that batch of magma (intrusion or eruption), then this process may have a bearing upon mineralization.

For example, the mature andesitic stratovolcano, Nevado del Ruiz, Colombia, is noted by Williams et al. (1998) to be the volcano that exhibits the greatest emission of "excessive gas" (including sulfur) of 50 "interesting" volcanoes for which they have compiled gas emission data. They note that although El Chichon and Pinatubo explosively released 7 and 20 million tons of SO$_2$, respectively, Nevado del Ruiz releases more gas per unit volume of magma erupted than any other volcano. They attribute the high emission rate of SO$_2$ to the high oxygen fugacity of the system. Others have proposed alternative explanations. For example, all recent eruptions of Nevado del Ruiz have been small plinian eruptions ($<$0.14 km^3) that have preserved the large

geothermal system that blankets the subvolcanic intrusions in the subsurface. Melson et al. (1990) record melt inclusion data that suggest that magma degassing is also feeding "the large well-developed geothermal system beneath Ruiz (Giggenbach et al. 1990)." In fact, they suggest that "only a small part" of the SO$_2$ that is being emitted by the volcano actually escapes to the atmosphere and is currently being measured. They propose that most of the degassed volatiles are being captured by the geothermal system. Underplated basaltic magma, which has periodically been replenishing the system over the last 2,000 years, is cited as a contributing source to the excess sulfur and the high level of seismicity and gas emissions. The possibility that the geothermal system at Nevado del Ruiz is producing a porphyry copper deposit at depth seems excellent.

What evidence exists that Bingham dacitic and monzonitic magmas may have been enriched in sulfur and other volatiles by similar processes? Keith et al. (1997) reported the existence of quenched (glass-bearing) latite dikes just external to the Bingham mineralization and alteration that contain abundant magmatic sulfides. The sulfides, in addition to being Ni-rich ($>$2 wt%) and Cu-rich (exsolved chalcopyrite), contain hundreds to thousands of ppm of Zn, As, Ag, and Pb and tens of ppm of Se, Mo, and Pd. It was noted that quenched dike margins tend to preserve the highest concentrations of magmatic sulfides. Work in progress (Stavast, personal communication 2001) is documenting the concentration and compositions of sulfides in these latite dikes adjacent to Butterfield Canyon and the Bingham deposit (Fig. 2). The outer few meters of these dikes contain from a few hundred to over 2,000 ppm sulfides by volume whereas the dike cores contain less than 10 ppm (similar to most volcanic rocks and intrusions). These data suggest that a sulfur-rich fluid, comparable in quantity to that present in Mount Pinatubo dacite, was present in the Bingham system. These dikes are also some of the few dikes in the Bingham system that are quenched enough to preserve amphibole coronas surrounding altered clots of biotite and olivine. It seems reasonable that intermixed or underplated lamprophyric magma, similar to the Bingham district melanephelinite, shoshonite or minette, was responsible for the apparently elevated S content in these latite dikes. Such inherited sulfur abundances are in line with the estimates of Carmichael and Ghiorso (1986) for mafic alkaline magmas with high oxygen fugacities for which they estimate sulfur concentrations of 2,000–4,000 ppm.

Trace-element modeling of late mineralized dikes at Bingham indicates that they were formed by mixing of about 10% melanephelinite magma and 90% felsic magma (Waite et al. 1997). If this ratio of magmas also applies to the source of the ore-forming volatiles and metals, then the melanephelinite magma would ultimately be responsible for contributing more than half of the sulfur and a significant portion of the copper and gold in the deposit.

In summary, what magmatic processes may have operated in the Bingham magmatic system as well as in other more ordinary porphyry-skarn magmatic systems? Three simple interrelated processes may be common (Keith et al. 1999):

1. Fractionation of calc-alkaline intermediate magma in a subvolcanic chamber to achieve saturation of water and other volatiles within significant volume of magma.
2. Interception or underplating of the subvolcanic intermediate magma by small volumes of sulfur-rich mafic magma.
3. Convection of volatile-rich magma from the base of the magma chamber to a subvolcanic cupola followed by volatile separation and descent of degassed magma (Lowenstern 1994; Shinohara et al. 1995).

A caveat of the above model is that overt mixing of mafic and intermediate magma need not occur in order for the mafic magma to crystallize and contribute a portion of its volatiles and metals to the overlying intermediate magma as it apparently did at Bingham. Some systems may receive significant additions of sulfurous gases and other volatiles as mafic magmas simply underplate and crystallize. However, this recurrent addition of volatiles to the dominant volume calc-alkaline magma may aid the process of convection and volatile collection as well as the final inventory of metals and sulfur in the deposit.

References

Allegre CJ, Hart SR, Minster JF (1983) Chemical structure and evolution of the mantle and continents determined by inversion of Nd and Sr isotopic data. I, Theoretical methods. Earth Planet Sci Lett 66:177–190

Armstrong RL, Ekren EB, McKee EH, Noble DC (1969) Space–time relations of Cenozoic silicic volcanism in the Great Basin of the western United States. Am J Sci 267:478–490

Atkinson WW Jr, Einaudi MT (1978) Skarn formation and mineralization in the contact aureole at Carr Fork, Bingham, Utah. Econ Geol 73:1326–1365

Babcock RCJr, Ballantyne GH, Phillips CH (1995) Summary of the geology of the Bingham district, Utah. In: Pierce FW, Bolm JG (eds) Porphyry copper deposits of the American Cordillera: Tucson, Arizona. Geol Soc Digest 20:316–335

Ballantyne GH, Smith TW, Redmond PB (1997) Distribution and mineralogy of gold and silver in the Bingham Canyon porphyry copper deposit, Utah. Soc Econ Geol Guidebook 29:147–153

Barr DL (1993) Time, space and composition patterns of middle Cenozoic mafic to intermediate composition lava flows of the Great Basin, western USA. MSc Thesis, Brigham Young University, Provo, Utah

Best MG, Christiansen EH (1991), Limited extension during peak Tertiary volcanism, Great Basin of Nevada and Utah. J Geophys Res 96:13509–13528

Best MG, Heinage LF, Adams JAS (1968) Mica peridotite, wyomingite, and associated potassic igneous rocks in northeastern Utah. Am Mineral 53:1041–1048

Blatter DL, Charmichael ISE (1998) Plagioclase-free andesites from Zitacuaro (Michoacan), Mexico: petrology and experimental constraints. Contrib Mineral Petrol 132:121–138

Boutwell JM (1905) Economic geology of the Bingham mining district, Utah. US Geol Surv Prof Pap 38:71–385

Carmichael ISE (1991) The redox state of basaltic and silicic magmas: a reflection of their source regions? Contrib Mineral Petrol 106:129–141

Carmichael ISE, Ghiorso MS (1986) Oxidation–reduction relations in basic magma: a case for homogenous equilibria. Earth Planet Sci Lett 78:200–210

Christiansen EH, Keith JD (1996) Trace element systematics in silicic magmas: a metallogenic perspective. In: Wyman D (ed) Trace element geochemistry of volcanic rocks: applications for massive sulphide exploration. Geol Assoc Can Short Course Notes 12:115–151

Christiansen EH, Keith JD (2000) Magmatic processes in the generation of porphyry copper deposit: the view provided by volcanic rocks in the Bingham district, Utah. Geol Soc Am Abstr Program 32:A51

Christiansen EH, Sheridan MF, Burt DM (1986) Geology and geochemistry of Cenozoic topaz rhyolites from the Western United States. Geol Soc Am Spec Pap 205

Constenius KW (1996) Late Paleogene extensional collapse of the Cordilleran Foreland fold and thrust belt. Geol Soc Am Bull 108:20–39

Deino A, Keith JD (1997) Ages of volcanic and intrusive rocks in the Bingham mining district, Utah. Soc Econ Geol Guidebook 29:91–100

Dilles JH, Proffet JM (1995) Metallogenesis of the Yerington Batholith, Nevada. In Pierce FW, Bolm JG (eds) Porphyry copper deposits of the American Cordillera. Ariz Geol Soc Digest 20:306–315

Esperanca S, Holloway JR (1987) On the origin of some mica-lamprophyres: experimental evidence from a mafic minette. Contrib Mineral Petrol 95:207–216

Evans NJ, Gregoire DC, Grieve RAF, Goodfellow WD, Veizer J (1993) Use of platinum-group elements for impactor identification: terrestrial impact craters and Cretaceous–Tertiary boundary. Geochim Cosmochim Acta 57:3737–3748

Farmer GL, DePaolo DJ (1983) Origin of Mesozoic and Tertiary granite in the western United States and implications for pre-Mesozoic crustal structure: Nd and Sr isotopic studies in the geocline of the northern Great Basin. J Geophys Res 88:3379–3401

Francis D, Ludden J (1995) The signature of amphibole in mafic alkaline lavas, a study in the northern Canadian Cordillera. J Petrol 36:1171–1191

Ghiorso M, Sack RO (1995) Chemical mass transfer in magmatic processes. IV A revised and internally consistent thermodynamic model for the interpolation and extrapolation of liquid–solid equilibria in magmatic systems at elevated temperatures and pressures. Contrib Mineral Petrol 119:197–212

Giggenbach WF, Garcia PN, Londono CA, Rodriguez VLA, Rojas GN, Calvache VML (1990) The chemistry of fumarolic vapor and thermal spring discharges from Nevado del Ruiz volcanic–magmatic–hydrothermal system, Colombia, J Volcanol Geotherm Res 41:13–40

Gilluly J (1932) Geology and ore deposits of the Stockton and Fairfield Quadrangles, Utah. US Geol Soc Prof Pap 173

Gustafson LB (1979) Porphyry copper deposits and calc-alkaline volcanism. In: McElhinney MW (ed) The Earth: its origin, structure, and evolution. Academic Press, London, pp 427–468

Hartmann G, Wedepohl KH (1990) Metasomatically altered peridotite xenoliths from the Hessian Depression (northwest Germany). Geochim Cosmochim Acta 54:71–86

Hattori K (1993) High-sulfur magma, a product of fluid discharge from underlying mafic magma: evidence from Mount Pinatubo, Philippines. Geology 21:1083–1086

Hattori KH, Keith JD (2001) Contribution of mafic melt to porphyry copper mineralization: evidence from Mount Pinatubo, Philippines, and Bingham deposit, Utah. Miner Deposita (in press)

Hintze LF (1988) Geologic history of Utah. Brigham Young University, Geol Studies Special Publication 7

Hunt JP (1977) Porphyry copper deposits. In: Volcanic processes in ore genesis: joint meeting of the Geological Society of London, Volcanic Studies Group, and the Institution of Mining and Metallurgy, London

Inan E, Einaudi MT (2000) Evolution toward high sulfidation in the uppermost contact aureole of the Bingham porphyry Cu–Au–Mo deposit, Utah. Geology and ore deposits 2000: the Great Basin and Beyond Symposium Proceedings, vol 1, p A3

Keith JD, Christiansen EH (1993) The genesis of giant porphyry molybdenum deposits. Soc Econ Geol, Giant Ore Deposits Spec Publ 2:385–415

Keith JD, Whitney JA, Hattori K, Ballantyne GH, Christiansen EH, Barr DL, Cannan TM, Hook CJ (1997) The role of magmatic sulfides and mafic alkaline magmas in the Bingham and Tintic mining districts, Utah. J Petrol 38:1679–1690

Keith JD, Christiansen EH, Maughan DT, Waite KA (1998) The role of mafic alkaline magmas in felsic porphyry-Cu and Mo systems. In: Lentz DR (ed) Mineralized "intrusion related" skarn systems. Mineral Assoc Can Short Course 26:211–243

Keith JD, Pulsipher T, Maughan DT, Waite KA, Christiansen EH, Tingey DG (1999) New developments in the geological understanding of magmatic processes that generate porphyry and associated ore deposits. In: New developments in the geological understanding of some major ore types and environments, with implications for exploration. Prospectors and Developers Association of Canada Short Course Proceedings, pp 47–63

Laes DYM, Krahulec KA, Ballantyne GH (1997) Geologic map of the Oquirrh Mountains, Utah, plate 1, scale 1:62,500. Soc Econ Geol Guidebook 29

Lanier G, John EC, Swensen AJ, Reid J, Bard CE, Caddey SW, Wilson JC (1978a) General geology of the Bingham mine, Bingham Canyon, Utah. Econ Geol 73:1228–1241

Lanier G, Raab WJ, Folsom RB, Cone S (1978b) Alteration of equigranular monzonite, Bingham mining district, Utah. Econ Geol 73:1270–1286

Larocque ACL, Stimac JA, Keith JD, Huminicki MAE (2000) Evidence for open behavior in immiscible Fe–S–O liquids in silicate magmas: implications for contributions of metals and sulfur to ore-forming fluids. Can Mineral 38:1233–1249

Le Bas MJ (1989) Nephelinitic and basanitic rocks. J Petrol 30:1299–1312

Le Maitre RW (1989) A classification of igneous rocks and glossary of terms. Blackwell, Oxford

Lindgren W (1924) Contact metamorphism at Bingham, Utah. Geol Soc Am Bull 35:507–534

Lowenstern JB (1994) Dissolved volatile concentrations in an ore-forming magma. Geology 22:893–896

Maughan DT (2001) Mafic to intermediate alkaline rocks of the Bingham district, Utah. MSc Thesis, Brigham Young University, Provo, Utah

Maughan DT, Keith JD, Pulsipher T, Tingey DG, Dorais MJ (1999) Eocene alkaline magmatism in north-central Utah and potential relationship to mineralization. Geol Soc Am Abstr Program 31:A405

McDonough WF, Sun SS (1995) The composition of the Earth. Chem Geol 120:223–253

Melker MD, Geissman JW (1997) Paleomagnetism of the Oquirrh Mountains and implications for the Cenozoic structural history of the easternmost Great Basin. Soc Econ Geol Guidebook 29:101–112

Melson WG, Allan JF, Jerez DR, Nelen J, Calvache ML, Williams SN, Fournelle J, Perfit M (1990) Water contents, temperature, and diversity of the magmas of the catastrophic eruption of Nevado del Ruiz, Colombia, November 13 1985. J Volcanol Geotherm Res 41:97–126

Michard A, Gurriet P, Soudant M, Albarede F (1985) Nd isotopes in French Phanerozoic shales: external vs. internal aspects of crustal evolution. Geochim Cosmochim Acta 49:601–610

Moore WJ (1973) Igneous rocks in the Bingham mining district, Utah. US Geol Soc Prof Pap 629-B

Moore WJ, McKee EH (1983) Phanerozoic magmatism and mineralization in the Tooele 1×2° quadrangle, Utah. Geol Soc Am Mem 157:183–190

Moore WJ, Lanphere MA, Obradovich JD (1968) Chronology of intrusion, volcanism, and ore deposition at Bingham, Utah. Econ Geol 63:612–621

Müller D, Groves DI (1993) Direct and indirect associations between potassic igneous rocks, shoshonites and gold–copper deposits, vol B. Ore Geology Reviews no 8. Elsevier, Amsterdam, pp 383–406

Müller D, Groves DI (2000) Potassic igneous rocks and associated gold–copper mineralization, 3rd edn. Springer, Berlin Heidelberg New York

Munoz JL (1981) F-OH and Cl-OH exchange in micas with applications to hydrothermal ore deposits. Mineral Soc Am Rev Mineral 13:469–493

Nakamura N (1974) Determinations of REE, Ba, Fe, Mg, Na and K in carbonaceous and ordinary chondrites. Geochim Cosmochim Acta 38:757–773

Parry WT, Wilson PN, Jasumback MD, Heizler MT (1997) Clay mineralogy and $^{40}Ar/^{39}Ar$ dating of phyllic and argillic alteration at Bingham canyon, Utah. Soc Econ Geol Guidebook 29:245–274

Phillips CH, Smith TW, Harrison ED (1997) Alteration, metal zoning, and ore controls in the Bingham Canyon porphyry Cu deposits, Utah. Soc Econ Geol Guidebook 29:133–145

Presnell RD (1992) Local and regional geology of the Oquirrh Mountains. In: Wilson JR (ed) Field guide to geologic excursions in Utah and adjacent areas of Nevada, Idaho, and Wyoming, Utah. Geological Survey Miscellaneous Publications 92-3, Salt Lake City, pp 292–306

Presnell RD (1997) Structural controls on the plutonism and metallogeny in the Wasatch and Oquirrh Mountains, Utah. Soc Econ Geol Guidebook 29:1–14

Pulsipher T (2000) The correlation of Eocene extrusive block and ash flows to intrusions at the Bingham copper porphyry system, Utah. MSc Thesis, Brigham Young University, Provo, Utah

Redmond PB, Einaudi MT (2000) The relationship between gold and copper in the Bingham Canyon porphyry deposit. Geology and ore deposits 2000. the Great Basin and Beyond Symposium Proceedings 1, p A3

Righter K, Carmichael ISE (1996) phase equilibria of phlogopite lamprophyres from western Mexico: Biotite–liquid equilibria and P–T estimates for biotite-bearing igneous rocks. Contrib Mineral Petrol 123:1–21

Roberts RJ, Crittenden MD Jr, Tooker EW, Morris HT, Hose RK, Cheney TM (1965) Pennsylvanian and Permian basins in northwestern Utah, northwestern Nevada, and south-central Idaho. Am Assoc Petrol Geol Bull 49:1926–1956

Rock NMS (1991) Lamprophyres. Blackie and Sons, New York

Severinghaus J, Atwater T (1990) Cenozoic geometry and thermal state of the subducting slabs beneath western North America. Geol Soc Am Mem 176:1–22

Shinohara H, Kazahaya K, Lowenstern JB (1995) Volatile transport in a convecting magma column: implications for porphyry Mo mineralization. Geology 23:1091–1094

Stacy JS, Zartman RE, Nkomo IT (1968) A lead isotope study of galenas and selected feldspars from mining districts in Utah. Econ Geol 63:796–814

Tingey DG, Christiansen EH, Best MG, Ruiz J, Lux DR (1991) Tertiary minette and melanephelinite dikes, Wasatch plateau, Utah: records of mantle heterogeneities and changing tectonics. J Geophys Res 96:13529–13544

Tomlinson DH Sr, Keith JD, Barr DL (2000) Correlation between redox states, source regions, and metallogenesis of middle Tertiary lavas of the western Unite States. In: Cluer JK, Price JG, Struhsacker EM, Hardyman RF, Morris CL (eds) Geology

and ore deposits 2000: the Great Basin and beyond. Geology Society of Nevada, pp 305–324

Waite KA, Keith JD, Christiansen EH, Whitney JA, Hattori K, Tingey DG, Hooks CJ (1997) Petrogenesis of the volcanic and intrusive rocks associated with the Bingham Canyon porphyry Cu–Au–Mo deposit, Utah. Soc Econ Geol Guidebook 29:69–90

Warnaars FW, Smith WH, Bray RE, Lanier G, Shafiqullah M (1978) Geochronology of igneous intrusions and porphyry copper mineralization at Bingham, Utah. Econ Geol 73:1242–1249

Williams SN, Burnham CW, Roggensack K (1998) Too much SO_2 – a problem of much recent interest: well, there may be simple controls! Geol Soc Am Program Abstr 30:A44

Wilson JC (1978) Ore fluid–magma relationship in a vesicular quartz latite porphyry dike at Bingham, Utah. Econ Geol 73:1287–1307